SECURITY CLASSIFICATION OF THIS PAGE DTIC

(2)

REPORT DOCUMENTATION PAGE

Form Approved OMB No 0704 0188

1a REPORT SEC: Unclass

AD-A237 505

2a SECURITY C

2b DECLASSIFI

1b. RESTRICTIVE MARKINGS

3. DISTRIBUTION/AVAILABILITY OF REPORT

Approved for public release and sale; its distribution is unlimited.

4 PERFORMING ORGANIZATION REPORT NUMBER(S)

Technical Report No. 104

5. MONITORING ORGANIZATION REPORT NUMBER(S)

6a NAME OF PERFORMING ORGANIZATION: Purdue University Department of Chemistry

6b. OFFICE SYMBOL (If applicable)

7a. NAME OF MONITORING ORGANIZATION: Division of Sponsored Programs Purdue Research Foundation

6c. ADDRESS (City, State, and ZIP Code): Purdue University Department of Chemistry West Lafayette, IN 47907

7b. ADDRESS (City, State, and ZIP Code): Purdue University West Lafayette, IN 47907

8a NAME OF FUNDING/SPONSORING ORGANIZATION: Office of Naval Research

8b. OFFICE SYMBOL (If applicable)

9 PROCUREMENT INSTRUMENT IDENTIFICATION NUMBER: Contract No. N00014-91-J-1409

8c ADDRESS (City, State, and ZIP Code): 800 N. Quincy Street Arlington, VA 22217

10 SOURCE OF FUNDING NUMBERS

PROGRAM ELEMENT NO.	PROJECT NO.	TASK NO	WORK UNIT ACCESSION NO

11. TITLE (Include Security Classification)

Cyclic Voltammetric Wave-Shapes for Microdisk Electrodes: Coupled Effects of Solution Resistance, Double-Layer Capacitance, and Finite Electrochemical Kinetics

12 PERSONAL AUTHOR(S)

L.K. Safford and M.J. Weaver

13a. TYPE OF REPORT	13b. TIME COVERED	14. DATE OF REPORT (Year, Month, Day)	15. PAGE COUNT
Technical	FROM ____ TO ____	May 31, 1991	

16 SUPPLEMENTARY NOTATION

17. COSATI CODES			18. SUBJECT TERMS (Continue on reverse if necessary and identify by block number)
FIELD	GROUP	SUB-GROUP	cyclic voltammograms at microdisk electrodes, double-layer capacitance, electrochemical kinetics, resistive/capacitance distortions

19. ABSTRACT (Continue on reverse if necessary and identify by block number)

Cyclic voltammograms at microdisk electrodes that account for the effects of solution resistivity ρ_Ω, double-layer capacitance, C_{dl}, and electrochemical kinetics have been simulated by using the explicit Hopscotch algorithm and a conformally mapped space-grid. The latter procedure, in particular, provides an efficient means of simulating voltammograms at slower potential scan rates where radial, rather than linear, diffusion predominates. Simulated voltammetric waveshapes as a function of scan rate are reported for systematic variations in ρ_Ω, C_{dl}, and the standard electrochemical rate constant k_s, both separately and together. The waveshape description utilizes both the anodic-cathodic potential peak separation, ΔE_p, and the halfwave potential for the forward scan in relation to the formal potential, $(E_h - E_f)$. The latter waveshape parameter is suitable for analyzing voltammograms where the influence of radial diffusion is sufficient to yield largely sigmoidal, rather than peaked, waveshapes. While the use of high scan rates enhances the effect of electrode kinetics upon the voltammetry, the deleterious coupled influence of ρ_Ω

20 DISTRIBUTION/AVAILABILITY OF ABSTRACT
☐ UNCLASSIFIED/UNLIMITED ☐ SAME AS RPT ☐ DTIC USERS

21. ABSTRACT SECURITY CLASSIFICATION

22a NAME OF RESPONSIBLE INDIVIDUAL

22b. TELEPHONE (Include Area Code)

22c. OFFICE SYMBOL

DD Form 1473, JUN 86 Previous editions are obsolete. SECURITY CLASSIFICATION OF THIS PAGE

19. (cont.)

and C_{dl} is also maximized under these conditions, especially for larger C_{dl} values. At slower scan rates, however, resistive/capacitance distortions are often attenuated greatly, while substantial kinetic information remains due to the enhanced mass transport associated with radial diffusion. The examination of voltammetric waveshapes over a wide range of scan rates, together with proper consideration of resistance/capacitance effects, therefore constitutes a desirable tactic for evaluating rapid electrode kinetics using microdisk electrodes. Representative simulation results are provided as a guide to such procedures, and as a means of assessing the degree of error involved if resistance/capacitance effects are neglected.

DISCLAIMER NOTICE

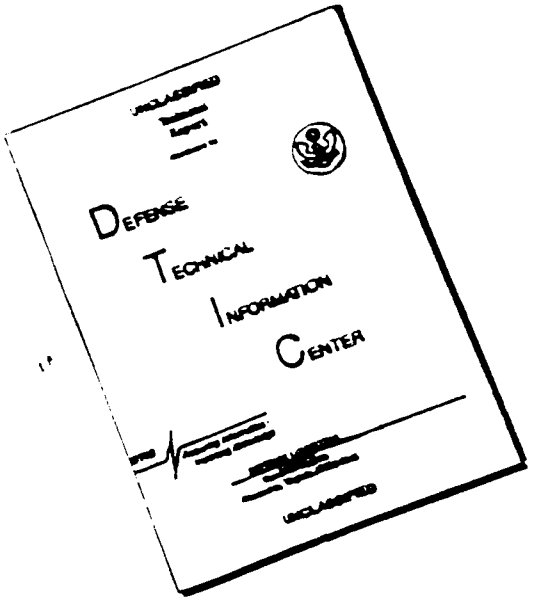

THIS DOCUMENT IS BEST QUALITY AVAILABLE. THE COPY FURNISHED TO DTIC CONTAINED A SIGNIFICANT NUMBER OF PAGES WHICH DO NOT REPRODUCE LEGIBLY.

OFFICE OF NAVAL RESEARCH

Contract No. N00014-91-J-1405

Technical Report No. 104

Cyclic Voltammetric Wave-Shapes for Microdisk Electrodes: Coupled Effects of Solution Resistance, Double-Layer Capacitance, and Finite Electrochemical Kinetics

by

L.K. Safford and M.J. Weaver

Prepared for Publication

in the

Journal of Electroanalytical Chemistry

Purdue University

Department of Chemistry

West Lafayette, Indiana 47907

May 1991

Cyclic Voltammetric Wave-Shapes for Microdisk Electrodes: Coupled Effects of Solution Resistance, Double-Layer Capacitance, and Finite Electrochemical Kinetics

Lance K. Safford and Michael J. Weaver

Department of Chemistry, Purdue University

West Lafayette, Indiana 47907, USA

J. Electroanal. Chem.

submitted December 10, 1990

revised March 1, 1991

ABSTRACT

Cyclic voltammograms at microdisk electrodes that account for the effects of solution resistivity ρ_Ω, double-layer capacitance, C_{dl}, and electrochemical kinetics have been simulated by using the explicit Hopscotch algorithm and a conformally mapped space-grid. The latter procedure, in particular, provides an efficient means of simulating voltammograms at slower potential scan rates where radial, rather than linear, diffusion predominates. Simulated voltammetric waveshapes as a function of scan rate are reported for systematic variations in ρ_Ω, C_{dl}, and the standard electrochemical rate constant k_s, both separately and together. The waveshape description utilizes both the anodic-cathodic potential peak separation, ΔE_p, and the halfwave potential for the forward scan in relation to the formal potential, $(E_{1/2} - E_f)$. The latter waveshape parameter is suitable for analyzing voltammograms where the influence of radial diffusion is sufficient to yield largely sigmoidal, rather than peaked, waveshapes. While the use of high scan rates enhances the effect of electrode kinetics upon the voltammetry, the deleterious coupled influence of ρ_Ω and C_{dl} is also maximized under these conditions, especially for larger C_{dl} values. At slower scan rates, however, resistive/capacitance distortions are often attenuated greatly, while substantial kinetic information remains due to the enhanced mass transport associated with radial diffusion. The examination of voltammetric waveshapes over a wide range of scan rates, together with proper consideration of resistance/capacitance effects, therefore constitutes a desirable tactic for evaluating rapid electrode kinetics using microdisk electrodes. Representative simulation results are provided as a guide to such procedures, and as a means of assessing the degree of error involved if resistance/capacitance effects are neglected.

Applications of cyclic voltammetry at microdisk electrodes for the evaluation of the rates of heterogeneous charge-transfer reactions,[1-11] as well as of homogeneous chemical processes [4,8,9,12-19] have become common in recent years. The minute double-layer capacitance seen at microelectrodes facilitates the use of extremely high potential scan rates without incurring extreme distortions of the voltammogram.[1-6,20] In the slow scan limit, a well-defined steady state response can be seen, whereby the diffusion layer is substantially larger than the electrode dimensions. This yields relatively efficient hemispherical diffusion to and from the electrode surface.[10,11,21-28]

Perhaps the most widely heralded feature of microelectrode voltammetry is the smaller degree of distortion due to solution resistance as compared with conventional-sized electrodes.[29] This property enables electrochemical reactions to be examined voltammetrically in extremely resistive media.[2,8,30-37] However, it should be stressed that while the use of microelectrodes can reduce the severity of resistive distortions, they cannot eliminate them. It is therefore important to examine carefully the remaining resistance-induced distortions in microelectrode voltammetry. This is especially important in the measurement of electrochemical kinetics, where the distorting effects of solution resistance can easily be attributed mistakenly to slow electrode kinetics.

These effects of solution resistance have been modeled previously assuming semi-infinite linear diffusion.[1,38-40] At microelectrodes, however, the attainment of this diffusion condition requires relatively high voltammetric scan rates. Resistive and migratory effects at microelectrodes under steady-state conditions, accessed at slow potential scan rates, have also been examined.[32,34,41,42] While semi-analytic solutions are available for these limiting regimes, digital simulation techniques are obligatory in the

intermediate case. Heinze considered previously the effects of finite electrode kinetics for the latter circumstances.[21,22] Aoki et al have investigated linear sweep voltammetry at microdisks in the reversible case,[23] and Zoski and co-workers have developed new analysis methods of "near-steady-state" voltammograms.[43] However, the effects of solution resistance and electrode capacitance on voltammetric waveshapes in the intermediate region have not been addressed.

In a recent preliminary note,[44] we employed the explicit Hopscotch algorithm[45,46] as developed for electrochemical applications[47-49] to simulate cyclic voltammetric waveshapes at microdisk electrodes. We examined the combined effects of resistance and electrode kinetics upon voltammetric peak separations. In the present article, we utilize the "conformal map" algorithm for disk electrodes developed by Michael et al[50] to present a more comprehensive and detailed report on this topic. Our major objective is to provide a means of diagnosing and assessing quantitatively the effects of solution resistance and electrode capacitance upon the evaluation of standard electrochemical rate constants, k_s, using microelectrode cyclic voltammetry.

Computational Methods

The results presented in this paper were generated by a finite difference algorithm modeling the diffusion to a disk electrode inlaid flush with a planar insulator during a cyclic voltammetric experiment. Thus, the diffusion equation that must be solved is

$$\frac{1}{D_i}\frac{dc}{dt} = \frac{\partial^2 c_i}{\partial r^2} + \frac{1}{r}\frac{\partial c_i}{\partial r} + \frac{\partial^2 c_i}{\partial z^2} \qquad (1)$$

where r and z are the directions parallel to and normal to the electrode surface, and c_i and D_i are the concentration and diffusion coefficient of redox species i. All results assume semi-infinite diffusional fields, with the reference electrode placed at infinity. The electron-transfer process:

$$Ox + ne^- = Red \qquad (2)$$

is modeled at the electrode surface. The diffusion coefficients of Ox and Red are assumed here to be equal. The initial concentration of Ox is zero, the solution containing only Red; with the initial potential scan being in the positive direction.

The simulation can be implemented in cylindrical coordinates with exponentially expanding space grids along each axis. This involves solving simultaneously the flux equation for the first layer of solution above the electrode surface and the Butler-Volmer kinetic relation (Eqs. 3 and 4, respectively):

$$\frac{\partial C_i}{\partial Z} = (C_i^{z=\Delta z} - C_i^{z=0})/\Delta z \qquad (3)$$

$$\frac{\partial C_i}{\partial Z} = X_0 \left[C_O^{z=0} \exp(-\alpha \frac{nF}{RT} \Delta E) - C_R^{z=0} \exp((1-\alpha)\frac{nF}{RT} E\Delta) \right] \qquad (4)$$

where α is the cathodic transfer coefficient (taken here as 0.5), ΔE is the difference between the applied and the formal potential, and X_0 is proportional to the standard hetergeneous rate constant. When solved simultaneously for the flux, we obtain

$$\frac{\partial C}{\partial Z} = \frac{\exp(-\alpha \frac{nF}{RT} \Delta E)\ C_0^{z=0} - \exp[(1-\alpha)\frac{nF}{RT} C_R^{z=0}]}{X_0^{-1} + \Delta Z\ (\exp(-\alpha \frac{nF}{RT} \Delta E) + \exp((1-\alpha)\frac{nF}{RT} \Delta E))} \qquad (5)$$

This relation is then used at each time step to determine the flux to the electrode surface. (For more details see ref. 47). The two dimensional nature of this problem requires a very efficient algorithm to avoid expending extreme amounts of computer time. The algorithm used initially here was the explicit 'fast' Hopscotch method.[48,49]

Such direct solution of Eq. (1) even by the computationally efficient Hopscotch algorithm unfortunately becomes cumbersome when nonlinear diffusion predominates. However, Michael et al[50] have shown that a coordinate transform

to a space conforming to the shape of the diffusion layer at the electrode ("conformal map") and subsequent solution by Hopscotch results in an algorithm which can be dramatically more efficient than evaluating Eq. (1) in cylindrical space. Most data presented here were obtained by means of the conformal map procedure, although the conventional Hopscotch method outlined above was found to be valuable for checking its reliability. The former procedure was implemented as follows. Equations (6) and (7) are the relations for transformation from cylindrical coordinates to the conformal space, and Eq. (8) is the conformal transform of Eq. (1):

$$r = \cos(\theta)\cosh(\Gamma) \tag{6}$$

$$z = \sin(\theta)\sinh(\Gamma) \tag{7}$$

$$\frac{dc_i}{dt} = \sigma_i^2[\sin^2\theta + \sinh^2\Gamma]^{-1}\left[\frac{\partial^2 c_i}{\partial\theta^2} + \frac{\partial^2 c_i}{\partial\Gamma^2} - \tan(\theta)\frac{\partial c_i}{\partial\theta} + \tanh(\Gamma)\frac{\partial c_i}{\partial\Gamma}\right] \tag{8}$$

and

$$\sigma = (D_i\, RT/nF\nu a^2)^{1/2} \tag{9}$$

where a is the radius of the electrode, ν is the scan rate, and θ and Γ are the axes of the conformal space.[50] Our implementation of this simulation uses the same dimensionless variables and boundary conditions described in ref. 50 with the addition of parameters for solution resistance and double-layer capacitance.

The dimensionless parameters describing solution resistance, R_s, and double-layer capacitance, C_{dl}, are given in Eqs. (10) and (11), respectively:

$$\rho' = 4nFaDc^\circ(nF/RT)\,R_s \tag{10}$$

$$\gamma' = C_{dl}/(4nFaDc^\circ) \tag{11}$$

These quantities are related to the more common dimensionless parameters ρ, γ[38,39] employed in linear diffusion problems by

$$\rho = \rho'\pi/(4\sigma) \tag{12}$$

$$\gamma = 4\gamma'\sigma/\pi \tag{13}$$

In the course of our use of this approach, we have made two useful observations about the method itself. In ref. 50, it was noted that the maximum Γ-value, Γ_{max}, necessary to contain the diffusion layer within the simulational grid was determined empirically. We have found that this need not be the case. The appropriate value of Γ_{max} can be determined readily from

$$\Gamma_{max} = \ln (x + (x^2 - 1)^{1/2}) \tag{14}$$

where

$$x = 1.0 + 6.0 (r_{max}\sigma^2)^{1/2} \tag{15}$$

and where τ is the dimensionless time of the experiment. These relations can be understood by noting that Eq. (15) is a modified version of the traditional "$6.0(Dt)^{1/2}$ rule" which is used to determine the thickness of the diffusion layer. The first term on the right-hand-side of Eq. (15) accounts for the electrode radius, which has a value of unity in dimensionless cylindrical coordinates. Equation (14) then is simply a rearrangement of Eq. (6) where $\theta = 0$, i.e., at the edge of the electrode. We have found that when using Γ_{max} values generated by Eqs. (14) and (15), the simulation generally utilizes 95-98% of its allotted space.

The second observation was made while checking the accuracy of the algorithm. To do this, we input a small σ value, 1×10^{-4}, so to approximate semi-infinite linear diffusion. The result obtained with a grid size of 20 x 200 elements, as suggested in ref.50, did not agree with that obtained from conventional theory.[51,52] We found that as $\sigma \to 0$, the resolution along the Γ-axis must be increased in order to faithfully represent the diffusion profile. Figure 3 of ref.50 serves to explain further this point. In fact, for $\sigma = 1 \times 10^{-4}$, the grid size necessary to observe a result within 1% of that obtained assuming linear diffusion was 20 x 4000. Clearly, when simulating voltammograms with small σ-values, care must be taken to insure correctness of the result, and definitely, for very small values of σ, one would be foolish to use this method. In this regime, however, the more conventional

simulation methods are readily applicable.

Simulation of voltammograms when solution resistance, R_s, is non-zero is somewhat more complex. Under these conditions, the passage of current, i, generates a variable potential drop, iR_s, within the solution so that the potential across the double layer, E_{dl}, no longer varies linearly with time. The consequences of solution resistance are significant from a simulational standpoint; for now both potential and current are unknown and interdependent. Thus, a root-finding algorithm must be employed to determine the value of E_{dl}, consistent with the current being passed. In our modification of the conformal map to account for resistance, several different algorithms were tested. A simple binary bisector worked consistently, but increased computational time unacceptably. The fastest root-finding algorithm tested, a Newton-Raphson procedure[56], suffered from stability problems in the presence of large resistances and capacitances. The Van Wijngaarden-Dekker-Brent algorithm[56], however, provided sufficient stability and reasonable computational efficiency, and was used in all simulations presented here that involve non-zero resistance.

Three different computer systems were used to generate the results in this study. A Zenith 80386-based computer employing NDP Fortran-386, a Digital Equipment Corporation VAX 8800 running Ultrix, and a CDC Cyber-205 utilizing VSOS were all employed here. All calculations were performed using 64-bit precision. Identical test programs were processed on all three systems to check machine-independence of the results.

RESULTS AND DISCUSSION

Electrode Kinetics

The most convenient and common means of evaluating rate constants for quasi-reversible electrode reactions using cyclic voltammetry involves measuring the cathodic-anodic peak separations, ΔE_p, as a function of the

potential scan rate, ν.[51,52] Under the condition of semi-infinite linear diffusion, ΔE_p for immeasurably large k_s values will be independent of ν and equal to 2.2 RT/nF.[53] The observation of ΔE_p values that are larger and that increase with increasing scan rate provides a simple and well-known means of evaluating k_s[53], at least in the absence of significant distortion due to resistive effects.[38,39]

At a microdisk electrode, however, the variation in experimental timescale associated with changes in sweep rate serves to modify the nature of diffusional transport to the electrode. At slow scan rates, diffusional transport is predominantly radial, yielding the known steady state response of microdisk electrodes.[29] At sufficiently short timescales (i.e., at fast scan rates), microdisks behave identically to more conventionally sized electrodes exhibiting linear diffusion.[1] This varying diffusional character at microdisk electrodes causes the value of ΔE_p to depend significantly upon scan rate even in the absence of sluggish electrode kinetics or solution resistance.[21,22,50]

The situation in the presence of finite electrode kinetics, yet in the absence of solution resistance, is illustrated in Fig. 1, in the form of plots of ΔE_p versus log ($\nu^{-1/2}$). The results displayed were simulated assuming the following conditions: a = 5×10^{-4} cm, (dashed traces), 5×10^{-3} cm (solid traces), D = 1×10^{-5} cm^2 s^{-1}, n = 1, T = 298K. The sequence of curves displayed for both electrode radii correspond to differing values of k_s. The lowest curves in each set refer to the "reversible limit", i.e., for $k_s \rightarrow \infty$, and the highest curves to k_s = 0.2 cm s^{-1} (see the figure caption for other details). At a given sweep rate, ΔE_p increases as k_s decreases- a well known result. Less familiar, however, are the progressive increases in ΔE_p seen with *decreasing* scan rate for smaller ν values, both in the presence and absence of finite electrode kinetics. This tendency reflects the

increasing efficiency of radial diffusion as ν decreases.

Such scan rate-dependent diffusional character is an important consideration for the evaluation of electrode kinetics. One need only glance at the right-hand side of the plots for the larger electrode (dashed curves) in Figure 1 to discern this. Here there is a ca 30 mV displacement in ΔE_p between the curves for the slowest rate constant (0.2 cm s^{-1}, circles) and the reversible case (asterisks). If non-linear diffusion to the electrode surface is absent (as for the open circles and squares in Fig. 1), the corresponding values of ΔE_p differ by less than 10 mV at such slow scan rates. Thus, as the values of ν decrease into the regime where radial diffusion is increasingly prevalent, the concurrent increase in diffusional efficiency enhances the measurability of a given rate constant. Indeed, this phenomenon is the basis for the evaluation of electrode kinetics with steady-state microdisk voltammetry.[10,24,25] Particularly noticeable in Fig. 1 is the markedly larger effect of electrode kinetics upon ΔE_p for the smaller versus larger electrodes at slow scan rates, arising from the more efficient radial diffusion in the former case. At fast scan rates (i.e., the left-hand side of Fig. 1), however, the ΔE_p values for the two electrode sizes approach each other, reflecting the approach to the linear diffusion limit where the effect of electrode size on the mass transport characteristics will disappear.

Figure 2 displays the same type of information as Fig. 1, but in a dimensionless format so to be applicable to a wider variety of experimental situations. In this figure, the dimensionless peak separation as given by

$$\Delta\xi_p = (nF/RT)\ \Delta E_p \qquad (16)$$

is plotted against log σ, where σ is the diffusional parameter defined by Eq. (9). The dimensionless quantity σ provides a convenient yardstick of the diffusion-layer thickness in relation to the electrode size. For $\sigma \ll 0.1$,

the former is sufficiently smaller than the latter so that semi-infinite linear diffusion is approached. Increasing σ, as brought about by decreasing ν and/or a, enhances the importance of radial diffusion to the overall mass transport. For example, at a large electrode, say 2 mm radius, it would be necessary to use scan rates slower than ca 0.1 mV s^{-1} to observe significant radial diffusion character (assuming $D = 10^{-5}$ cm s^{-1}); clearly this is prevented by convective mass transport at such long timescales. Decreasing the electrode radius to 2×10^{-4} cm, however, will yield significant radial diffusion effects at scan rates below 100 V s^{-1}, well within the usual range of voltammetric timescales.

The bottom curve in Fig. 2 refers to the "reversible" case, (i.e. where $k_s \rightarrow \infty$). An empirical regression fit to this curve is given by

$$\Delta\xi_p = (5.44 \pm 0.084)\sigma + (2.21 \pm 0.027) \qquad (17)$$

These results agree well with Heinze's earlier simulations.[21] Note that $\Delta\xi_p$ increases progressively for larger σ values. For $\sigma \gtrsim 0.5$, however, the cathodic and anodic voltammetric peaks are sufficiently broad and ill-defined as to be barely discernable. Eventually a "steady-state" response is attained, consisting of the well-known sigmoid current-potential curves.[27,28] The nine upper curves in Fig. 2 were calculated for a sequence of decreasing electrochemical reactivities, as gauged by the conventional "heterogeneous kinetic parameter"[53]

$$\psi = \frac{(D_o/D_r)^{\alpha/2} k_s}{[D\pi(nF/RT)\nu]^{1/2}} \qquad (18)$$

where D_o and D_r are the diffusion coefficients of the oxidized and reduced redox forms.

The virtue of the dimensionless representation in Fig. 2 is that the numerical results are applicable to a range of electrode radii and scan rates.

Since each curve corresponds to a fixed ψ value, the ratio of k_s to ν remains constant. As the data sets in Fig. 2 are only a small representation of an infinite family of σ-ψ-$\Delta\xi_p$ curves, a convenient method of determining the value of ψ corresponding to given values of $\Delta\xi_p$ and of σ would be of merit. We have found that each of the curves in Fig. 2 can be fit to reasonable accuracy by an equation of the form of:

$$\Delta\xi_p = C_1 \exp\,(C_2 \log_{10}(\sigma)) + C_3 \tag{19}$$

where C_1, C_2, C_3 are fitting parameters unique to each value of ψ. Indeed, the solid traces in Figure 2 were obtained in such a manner. Moreover, the C_i coefficients each follow a reasonably simple function of $\log_{10}(\psi)$, as in Eq. (20-22):

$$C_1 = a_1\,(1 - \exp\,(-(a_2 + a_3\beta + a_4\beta^2 + \frac{a_4^2\beta^3}{3a_3}\,))) \tag{20}$$

where

$$a_1 = 12.87 \pm 0.1$$

$$a_2 = 1.07 \pm 0.03$$

$$a_3 = -1.13 \pm 0.06$$

$$a_4 = 0.65 \pm 0.06$$

and where $\beta = \log_{10}(\psi)$.

$$C_2 = a_5 + a_8\, a_6/((\beta - a_7)^2 + a_6^2) \tag{21}$$

where

$$a_5 = 2.127 \pm 0.007$$

$$a_6 = 0.70 \pm 0.05$$

$$a_7 = 0.092 \pm 0.12$$

$$a_8 = 0.51 \pm 0.05$$

$$C_3 = a_9 \exp(a_{10}\,\beta) + a_{11} \tag{22}$$

where

$$a_9 = 1.4 \pm 0.1$$

$$a_{10} = -1.43 \pm 0.07$$

$$a_{11} = 2.04 \pm 0.09$$

Given these three relations and experimental values for $\Delta\xi_p$ and σ, one can search over the interval of experimentally reasonable values of ψ until a curve fitting the $\Delta\xi_p$ value at the known σ value is obtained, rendering the desired ψ and hence the k_s value. Although only approximate, this is a convenient approach for estimating rate constants over a wide range of σ from peak separations.

An interesting feature of the curves in Fig. 2 is that their vertical displacement ($\Delta\xi_p$) from the reversible limit increases markedly as σ increases. This reflects the increased efficiency of mass transport, and hence a proportionately greater influence of electrochemical kinetics upon the voltammetric response, in the increasing presence of radial diffusion. Similar findings have been obtained by other workers.[9,10,37] The results in Fig. 2 therefore suggest that the most advantageous method of evaluating electrochemical kinetics with microelectrode cyclic voltammetry would be to choose conditions so to maximize σ, thereby making the diffusional transport faster relative to the electrode kinetics. It is, alas, not that simple. As already noted, the "peakedness" of the voltammogram also decreases under these conditions, making it increasingly difficult to identify accurately the peak potentials from experimental data. This point is illustrated in Fig. 3, which consists of simulated voltammograms for several values of σ, as indicated.

As an alternative to peak potential separations, the half-wave potential $E_{1/2}$ for the forward scan (i.e., the potential at which the current reaches one half the maximum value) can be utilized. While the separation between the $E_{1/2}$ values for the forward and reverse scans, $\Delta E_{1/2}$, may be employed in a fashion similar to ΔE_p values, one limitation is that $\Delta E_{1/2}$ approaches zero in the steady-state limit. A simple alternative is to use $E_{1/2}$ itself, most conveniently for the forward potential sweep, in relation to the formal poten-

tial E_{ξ}. The difference ($E_{\frac{1}{4}}$- E_{ξ}) can be utilized as a kinetically sensitive parameter *throughout* the regime where radial diffusion is important including the steady-state limit.

Figure 4 contains plots of ($E_{\frac{1}{4}}$-E_{ξ}) versus log ($\nu^{-\frac{1}{4}}$) for the same set of k_s values as in Fig. 1. The x-axis is extended, however, to smaller scan rates [i.e., larger log ($\nu^{-\frac{1}{4}}$) values] so to yield conditions approaching the steady-state limit. Inspection of Fig. 4 shows that the sensitivity of the voltammetry to electrode kinetics, as discerned by the displacement of ($E_{\frac{1}{4}}$-E_{ξ}) for a finite k_s value above the reversible ($k_s \rightarrow \infty$) curve, survives even to small scan rates. Similarly to Fig. 1, this results from the offsetting influences of the longer timescales and more efficient mass transport associated with smaller scan rates. Figure 5 displays the same type of information, but in a dimensionless format, as a plot of ($\xi_{\frac{1}{4}}$- ξ_{ξ}) versus log σ, where ($\xi_{\frac{1}{4}}$- ξ_{ξ}) = (nF/RT)($E_{\frac{1}{4}}$-E_{ξ}) (cf Fig. 2).

Solution Resistance

The presence of solution resistance has long been known to cause significant distortions to cyclic voltammograms, most notably to enlarge the ΔE_p values.[1,38,39] Unfortunately, the functional nature of this influence upon ΔE_p is often similar to that brought about by finite electrode kinetics. The unambiguous identification of kinetic and resistive effects in their simultaneous presence is therefore clearly important. While this issue has been the focus of several studies,[1,3] these have dealt only with the case of pure linear diffusion. Below, we provide some examples of the effects of resistance on voltammograms also influenced by the changing diffusional character of microdisk electrodes.

Newman[54] has shown that the resistance, R_s, for a disk electrode in isotropic media with the auxiliary and reference electrodes an infinite distance away is given by

$$R_s = \rho_\Omega / 4a \qquad (23)$$

where ρ_Ω is the solution resistivity. Although Eq. (23) shows that R_s will increase as the electrode radius decreases, this effect is more than offset by the diminished currents obtained under these conditions, yielding smaller iR_s potential drops. The current under conditions of linear diffusion ($\sigma = 0$) is proportional to the electrode area (and hence a^2), so that iR_s will decrease linearly with decreasing a. At the extreme of steady-state diffusion to a microdisk,[23] ($\sigma \rightarrow \infty$), the limiting current becomes proportional to the electrode radius, whereupon the iR_s drop is independent of electrode area (vide infra).[41,42] At finite non-zero values of σ, an intermediate situation will prevail.

While it has been common to neglect resistive effects in kinetic applications of microelectrode voltammetry, this is clearly a dangerous tactic. This point is illustrated straightforwardly in Fig. 6, as plots of ΔE_p versus log ($\nu^{-1/2}$) for various ρ_Ω values but in the absence of finite electrode kinetics (i.e., for $k_s \rightarrow \infty$). As before, the solid and dashed traces refer to 0.5 and 5 μm radius electrodes, respectively. The ρ_Ω values are selected so to span the values commonly encountered in organic solvent systems. Thus the increasing ρ_Ω values in Fig. 6 (from 200 to 2670 Ω cm) correspond to nitromethane, formamide, methylene chloride, ethanol, and tetrahydrofuran, each containing 0.1 M tetrabutylammonium perchlorate[55] (see figure caption for further details). The lowest curve in each set corresponds to $\rho_\Omega = 0$.

Comparison of Fig. 6 with Fig. 1 shows that the effect of solution resistance upon ΔE_p as a function of scan rate is qualitatively similar to that observed for finite electrode kinetics. Nevertheless, there are two noteworthy differences. Most strikingly, the effect of altering the electrode size at a given scan rate is qualitatively different. While the influence of solution resistance upon ΔE_p diminishes as the electrode radius decreases

(Fig. 6), the role exerted by electrode kinetics is enhanced under these conditions (Fig. 1). As noted above, the latter effect becomes increasingly important as the electrode size decreases, and hence the degree of radial diffusion increases. In addition, careful comparison of Figs. 1 and 6 reveals that even at the larger electrode the influence of electrode kinetics upon ΔE_p becomes greater relative to the corresponding effect of solution resistance as the scan rate decreases. This phenomenon also has its origin in the enhanced mass transport efficiency that ensues as the degree of radial diffusion is increased.

These comparisons also serve to emphasize the central role played by the electrode size in influencing the measurability of electrochemical kinetics in the face of distortions from solution resistance. The common tactic of increasing the scan rate can enhance greatly the effect of electrode kinetics upon ΔE_p, particularly if the degree of radial diffusion is small (i.e., the left-hand-side of Fig. 1). However, the effect of solution resistance upon ΔE_p also can increase markedly under these conditions, tending to negate the enhanced effect of electrode kinetics. By examining ΔE_p at lower scan rates, on the other hand, the effect of electrode kinetics relative to solution resistance can be enhanced dramatically if sufficiently small electrodes are employed so to provide efficient radial diffusion.

Similar arguments apply if half-wave potentials rather than peak separations are employed. Figure 7 is a plot of $(E_{\frac{1}{2}} - E_f)$ versus log $(\nu^{-\frac{1}{2}})$ for the same set of solution resistance values and other parameters as in Fig. 6. The effect of resistance is again seen to be minimized at low scan rates as well as for smaller electrodes. One additional point is evident upon comparing Fig. 7 with the corresponding plot for electrode kinetics in Fig. 4. While the sensitivity to electrode kinetics is maintained over a wide range of scan rates in the radial diffusion regime, the effect of resistance (if

significant) displays a similar invariance. Consequently, then, one must be careful to estimate the degree to which the known solution resistance should distort experimental voltammograms before asserting that ΔE_p and $E_{1/4}$ values that deviate from the "ideal reversible" limits signal the presence of measurable electrode kinetics.

With the aim of providing a more complete numerical picture of the effects of solution resistance on microdisk cyclic voltammetry, Figs. 8 and 9 display plots of $\Delta\xi_p$ and $(\xi_{1/4} - \xi_p)$ versus log σ for a series of values of the dimensionless resistance parameter, ρ [Eqs. (10), (12)]. A cursory examination of both figures reveals that the separation between the uppermost curve ($\rho = 10$) and the lowest curve ($\rho = 0$) increases as σ increases, i.e., from left to right. This is caused by the relative increase in current magnitude as σ increases, i.e., by the more efficient diffusion observed near steady-state conditions. The dimensionless format is designed to maintain the resistive drop constant relative to the scan rate in the linear diffusion limit. As a result of the increased diffusional efficiency encountered at lower scan rates, the magnitude of the resistive drop increases as the steady-state limit is approached. Fortunately, one is unlikely to encounter a situation where ρ is large for steady-state conditions, except for extremely high solution resistances such as are encountered in the absence of supporting electrolyte. In this case, however, Oldham has pointed out that Newman's isotropic condition is no longer valid, and the ohmic treatment of resistance is likewise inappropriate.[34]

The results discussed so far neglect the additional influence of double-layer capacitance, C_{dl}, on the voltammetric response. In the absence of significant effects from solution resistance, a constant non-zero capacitance will provide merely a background nonfaradaic current without altering the voltammetric waveshape. In the presence of solution resistance effects,

however, the electrode capacitance can yield additional voltammetric distortions since the time derivative of the double-layer potential, dE_{dl}/dt, and hence the nonfaradaic current, can vary substantially with potential even when C_{dl} is potential-independent.[8,40] This situation yields a close coupling between the voltammetric distortions arising from R_s and C_{dl}, in that the presence of the latter tends to enhance the effect of the former.

This point is illustrated in Figs. 10 and 11, in the form of plots of ΔE_p and $(E_{\frac{1}{4}} - E_{\frac{3}{4}})$, respectively, versus log $(\nu^{-\frac{1}{2}})$ (cf Figs. 6,7) for an electrode radius of 5 μm. The open and filled symbols refer to ρ_Ω values of 725 and 1800 Ω cm^{-1}, respectively. (These values were chosen since they are appropriate for voltammetry in the moderately resistive media methylene chloride and ethanol, respectively, both containing 0.1 M supporting electrolyte[55]). The trio of points in these two sets (circles, squares, and triangles) refer to C_{dl} values of 5, 15, and 25 μF cm^{-2}, respectively. These plots show the extent to which the presence of larger C_{dl} values accentuates the effect of solution resistance. At the highest scan rate (10^4 V s^{-1}) shown in Fig. 10, for example, increasing C_{dl} fivefold, from 5 to 25 μF cm^{-2}, increases ΔE_p to an extent similar to enhancing R_s by ca 2.5-fold, from 725 to 1800 Ω cm^{-1}. The relative importance of such C_{dl} effects, however, diminishes sharply towards smaller scan rates (Figs. 10, 11) as expected since the magnitude of the nonfaradaic currents is decreased under these conditions.

These results indicate that the use of high scan rates, often sought after as a means of evaluating rapid electrode kinetics, can be problematic for this purpose. Under conditions where solution resistance is known (or suspected) to distort significantly the voltammograms, it will often be necessary to account additionally for capacitance effects. A difficulty with the latter is that C_{dl} is inherently a surface-sensitive property, its mag-

nitude being determined by the interfacial structure composition (and even by electrode construction techniques[57]). In addition, significant capacitance contributions can arise from electrode leads and connections ("stray capacitance"). It is therefore important to evaluate carefully the occurrence and magnitude of such coupled resistance-capacitance effects.

Combination of Solution Resistance, Double-Layer Capacitance and Electrode Kinetics

Ideally, one would prefer to present a complete picture of the effects of resistance, capacitance and kinetics when they are simultaneously present. This undertaking, even in the linear diffusion limit, would be a formidable task. By including the scan rate-dependent diffusional character obtained at a microdisk, it becomes completely impractical! We nonetheless wish to provide a brief overview of the coupled effects that all these factors can exert on voltammetric wave shapes. To that end, we provide some specific examples of the combined effects of resistance, capacitance, and electrode kinetics. Included are some examples of the errors that can accrue if resistive and capacitive distortions are ignored in the evaluation of electrode kinetics.

The first example is contained in Figs. 12 and 13. These figures contain corresponding plots of ΔE_p and $(E_{1/4} - E_f)$, respectively, against log $(\nu^{-1/2})$. As before, the solid and dashed lines refer to 0.5 and 5 μm radius electrodes, respectively. Results are shown in Figs. 12 and 13 for a pair of solution resistances: 100 Ω cm (open symbols) and 1000 Ω cm (filled symbols). For both of these ρ_Ω values, data are shown for a relatively low and high k_s value, 0.2 cm s^{-1} (circles) and 5 cm s^{-1} (squares). The double-layer capacitance is fixed in each case at 5 μF cm^{-2}; other parameters are as utilized above.

As expected, the voltammetric responses at the larger electrode are

affected substantially more by solution resistance than those for the smaller electrode, especially at high scan rates. The degree to which solution resistance alters both ΔE_p and $E_{\frac{1}{4}}$, however, is dependent significantly on the extent to which electrode kinetics also affects these parameters. Thus the increase in ΔE_p obtained for a given k_s value by increasing ρ_Ω (discerned by comparing corresponding open and filled symbols in Fig. 12) is noticeably less for $k_s = 0.2$ cm s^{-1} than for 5 cm s^{-1}. In other words, the extent of additional resistive distortion upon ΔE_p tends to diminish somewhat for voltammograms that also feature the effects of more sluggish electrode kinetics. This coupling between the effects of solution resistance and electrode kinetics arises primarily from the diminution in the currents that result from slower kinetics. We also pointed out this non-additive nature of solution resistance and electrode kinetic effects upon ΔE_p in our preliminary communication.[44] Similar effects are also seen when $(E_{\frac{1}{4}} - E_{\frac{3}{4}})$ is utilized as the voltammetric parameter (Fig. 13).

A necessary consequence of this coupling between resistance and kinetic effects is that the additional effect of electrode kinetics upon ΔE_p and $(E_{\frac{1}{4}} - E_{\frac{3}{4}})$ tends to diminish somewhat in the presence of distortions from solution resistance. This situation emphasizes the need to select conditions, such as slower scan rates and smaller electrode radii, so that the effect of solution resistance is minimized or at least characterized.

One other feature of Fig. 13 worth mentioning here is that the displacement in $(E_{\frac{1}{4}} - E_{\frac{3}{4}})$ for each pair of curves corresponding to the different ρ_Ω values become not only insensitive to scan rate for small ν, but are also independent of the electrode radius under these conditions. Although this phenomenon does not appear to be particularly useful in the present context, it is in agreement with analytical predictions that refer to the steady-state limit.[41,42] As noted above, an additional complication wrought by the occur-

rence of significant voltammetric distortions from solution resistance is that the extent of this effect will also be dependent on the magnitude of the double-layer capacitance. Figures 14 and 15 contain plots in the same format as Figs. 12 and 13, respectively, that illustrate the effects of altering the double-layer capacitance, C_{dl}, from 5 $\mu F\ cm^{-2}$ (circles) to 25 $\mu F\ cm^{-2}$ (squares). Each of these curves in Figs. 14 and 15 refer to a rate constant of 0.2 cm s^{-1}. (The other symbolism and conditions are as in Figs. 12 and 13).

Inspection of Figs. 14 and 15 shows that variations in the double-layer capacitance as well as the solution resistance can exert a significant influence on both ΔE_p and $(E_{\frac{1}{2}} - E_f)$ in the presence of finite electrode kinetics, especially for larger electrodes and high scan rates. As before (Figs. 12, 13), the effects of C_{dl} and ρ_Ω on these parameters are strongly coupled. Thus increasing C_{dl} fivefold, from 5 to 25 $\mu F\ cm^{-2}$ for the larger ρ_Ω value 1000 Ω cm, increases ΔE_p at high scan rates to an extent comparable to the distortions incurred by such a large solution resistivity alone. Such effects incurred by altering ρ_Ω and/or C_{dl} at such large resistivities can easily be comparable to those incurred by substantial changes in k_s. At the highest ρ_Ω value and scan rates in Fig. 14, for example, the effect upon ΔE_p of increasing C_{dl} from 5 to 25 $\mu F\ cm^{-1}$ can be offset almost entirely by altering k_s by a similar factor, from 0.2 to 1 cm s^{-1}. Consequently, the reliable extraction of k_s under these conditions requires quantitative information on both ρ_Ω and C_{dl}. Such coupled effects provide a clear warning to the experimentalist attempting to evaluate rapid electrode kinetics by means of microelectrode voltammetry. The use of high scan rates and larger (ca 5 μm radius) electrodes, employed commonly for this purpose, are precisely the conditions for which the coupled distortions from solution resistance and electrode capacitance effects are most severe.

A further illustration of the deleterious influence of such factors upon the evaluation of electrode kinetics is given in Fig. 16. Simulated voltammograms were generated at a sequence of scan rates from 1.0 to 10^4 V s^{-1} for k_s values equal to 0.1, 0.2 and 0.5 cm s^{-1} (triangles, squares, and circles, respectively, in Fig. 16), with $a = 5$ μm, $\rho_\Omega = 200$ Ω cm^{-1}, and $C_{dl} = 10$ μF cm^{-2} (This solution resistivity, a "moderate" value, approximates that appropriate for methylene chloride containing 0.5 M tetraalkylammonium salt). Apparent estimates of k_s, k_s(app) were extracted from each of these voltammograms by using the procedure outlined above, but assuming that $\rho_\Omega = 0$. This procedure therefore mimics the common assumption that solution resistance effects can be neglected in microelectrode voltammetry. The degree of systematic error resulting from this neglect of solution resistance is displayed in Fig. 16 in the form of k_s(app)/k_s ratios plotted versus log ($\nu^{-1/2}$). Inspection of Fig. 16 shows that while k_s(app)/$k_s \approx 1$ for $\nu \leq 100$ V s^{-1}, this ratio diminishes systematically towards higher scan rates, especially for larger k_s. These results affirm that the neglect of solution resistance in the evaluation of k_s becomes increasingly serious at higher scan rates, k_s(app) estimates that are progressively smaller than the true values being recovered under these conditions.

A final, perhaps more visual, example of resistive effects upon the evaluation of electrode kinetics is contained in Figs. 17A and B. The former displays two sets of three cyclic voltammograms, simulated at a relatively high scan rate, 2500 V s^{-1}, and for the usual conditions considered here, with $a = 5$ μm, $C_{dl} = 10$ μF cm^{-2}, with solution resistivities of 0 (solid traces), 130 (dashed traces), and 720 Ω cm^{-2} (dotted traces). The latter two ρ_Ω values are appropriate for 0.1 M tetrabutylammonium perchlorate in acetonitrile and methylene chloride, respectively. The inner trio of voltammograms (i.e., with the smaller ΔE_p values) were calculated for $k_s \rightarrow \infty$, and

the outer trio refer to $k_s = 0.2$ cm s^{-1}. Examination of Fig. 17A shows that distinctly different voltammetric waveshapes are obtained for a given k_s value as the solution resistance is altered over this commonly encountered range. Indeed, the increased ΔE_p and related voltammetric distortions attending such alterations in the solution medium could easily be identified mistakenly as reflecting substantial solvent-induced variations in the electron-transfer rate constant.

Figure 17B contains corresponding cyclic voltammetric data as in Fig. 17A, but for a slower scan rate, 25 V s^{-1}. Only two curves are shown, corresponding again to $k_s \rightarrow \infty$ (solid trace) and $k_s = 0.2$ cm s^{-1} (dotted trace). Unlike the data at the faster scan rate, (Fig. 17A) the voltammograms in Fig. 17B simulated for the three ρ_Ω values are essentially coincident, i.e., the effect of solution resistance is negligible under these conditions. The influence of electrode kinetics is nonetheless still significant at the slower scan rate, as seen from the noticeable difference between the two voltammograms in Fig. 17B. Admittedly, however, the *degree* of kinetic information available under these conditions is clearly smaller than that gleaned for the fast scan rate in Fig. 17A, as discerned from the markedly greater increase in ΔE_p resulting from decreasing k_s in the latter case. Clearly, it is important to select measurement conditions where the desired degree of kinetic information is maintained while minimizing (or at least controlling) the known influence of coupled solution resistance/electrode capacitance effects.

Concluding Remarks

This study demonstrates that the reliable simulation of cyclic voltammograms at microdisk electrodes, even in the presence of substantial radial diffusion and with significant effects from both solution resistance and finite electrode kinetics, is computationally feasible by using a con-

formal space grid. This algorithm is sufficiently efficient that such simulations can be effectively generated on high performance personal computers. On faster computer systems, a variant of this algorithm could also be used to fit simulated voltammograms to experimental data in an interactive fashion, as is common for the case of linear diffusion.[1,3,4,6,8,12]

The present results show that the ability to evaluate rapid electrode kinetics can be impaired substantially at microdisk electrodes even in moderately resistive solvents. While the common tactic of employing high scan rates enhances the degree of kinetic information attainable, the deleterious influence of solution resistance can be sufficiently great under these conditions so to impair severely the extraction of reliable rate constant values. This difficulty is made more acute by the coupled influence of double-layer capacitance, which can act to magnify substantially the distorting influence of solution resistance at high scan rates.

In the light of these considerations, in order to extract reliable electrode kinetic data it is desirable to analyze microdisk voltammetric data obtained for a range of scan rates that also encompasses the regime where radial diffusion contributes importantly to the mass transport. Other than at the steady-state limit the analysis of this regime is, admittedly, computationally quite demanding. Nevertheless, the greater mass-transport efficiency engendered by radial diffusion acts to enhance the influence of electrode kinetics on the voltammetric waveshape relative to the undesired coupled effects exerted by solution resistance and double-layer capacitance. As a consequence, then, the careful examination of voltammograms over an appropriately large range of scan rates, together with the appropriate knowledge of ρ_Ω and C_{dl}, may be considered to be a prerequisite for the reliable extraction of electrochemical rate constants.

ACKNOWLEDGMENTS

We are grateful to Mark Wightman and Adrian Michael for supplying details of the conformal map algorithm. The implementation of the simulations was also aided substantially by discussions with Pat Santangelo and the late George McManis. This work is supported by the Office of Naval Research.

REFERENCES

1. D. O. Wipf, E. W. Kristensen, M. R. Deakin, R. M. Wightman, Anal. Chem., 60 (1988), 306.

2. J. O. Howell, R. M. Wightman, Anal. Chem., 56 (1984), 524.

3. C. P. Andrieux, D. Garreau, P. Hapiot, J. Pinson, J.-M. Savéant, J. Electroanal. Chem., 243 (1988), 321.

4. D. O. Wipf, R. M. Wightman, Anal. Chem., 60 (1988), 2460.

5. M. I. Montenegro, D. Pletcher, J. Electroanal. Chem., 200 (1986), 371.

6. C. P. Andrieux, D. Garreau, P. Hapiot, J.-M. Saveant, J. Electroanal. Chem., 248 (1988), 447.

7. A. M. Bond, T. L. E. Henderson, D. R. Mann, T. F. Mann, W. Thormann, C. G. Zoski, Anal. Chem., 60 (1988), 1878.

8. W. J. Bowyer, E. E. Engelman, D. H. Evans, J. Electroanal. Chem., 262 (1989), 67.

9. J. O. Howell, R. M. Wightman, J. Phys. Chem., 88 (1984), 3915.

10. K. B. Oldham, C. G. Zoski, A. M. Bond, D. A. Sweigart, J. Electroanal. Chem., 248 (1988), 467.

11. A. Russell, K. Repka, T. Dibble, J. Ghoroghchian, J. J. Smith, M. Fleischmann, C. H. Pitt, S. Pons, Anal. Chem., 58 (1986), 2961.

12. C. P. Andrieux, P. Hapiot, J.-M. Savéant, J. Phys. Chem., 92 (1988), 5987.

13. M. I. Montenegro, D. Pletcher, J. Electroanal. Chem., 248 (1988), 229.

14. C. A. Amatore, A. Jutand, F. Pflüger, J. Electroanal. Chem., 218 (1987), 361.

15. A. Fitch, D. H. Evans, J. Electroanal. Chem., 202 (1986), 83.

16. J. E. Baur, E. W. Kristensen, L. J. May, D. J. Wiedeman, R. M. Wightman, Anal. Chem., 60 (1988), 1268.

17. G. Denuault, M. Fleischmann, D. Pletcher, J. Electroanal. Chem., 280 (1990), 255.

18. M. Fleischmann, F. Lasserre, J. Robinson, J. Electroanal. Chem., 177 (1984), 115.

19. M. Fleischmann, F. Lasserre, J. Robinson, D. Swan, J. Electroanal. Chem., 177 (1984), 47.

20. C. Amatore, C. Lefrou, F. Pflüger, J. Electroanal. Chem., 270 (1989), 43.

21. J. Heinze, Ber. Bunsenges. Phys. Chem., 85 (1984), 1096.

22. J. Heinze, M. Störzbach, Ber. Bunsenges. Phys. Chem., 90 (1986), 1043.

23. K. Aoki, K. Akimoto, K. Tokuda, H. Matsuda, J. Osteryoung, J. Electroanal. Chem., 171 (1984), 219.

24. K. B. Oldham, J. C. Myland, C. G. Zoski, A. M. Bond, J. Electroanal. Chem., 270 (1989), 79.

25. A. M. Bond, K. B. Oldham, C. G. Zoski, J. Electroanal. Chem., 245 (1988), 71.

26. M. Fleischmann, S. Pons, J. Electroanal. Chem., 222 (1987), 107.

27. M. Fleischmann, J. Daschbach, S. Pons, J. Electroanal. Chem., 263 (1989), 189.

28. D. K. Cope, D. E. Tallman, J. Electroanal. Chem., 285 (1990), 79.

29. M. Fleischmann, S. Pons, D. R. Rolison, P. P. Schmidt, Ultramicroelectrodes Datatech Systems, Inc., (Morganton: 1987).

30. A. M. Bond, P. A. Lay, J. Electroanal. Chem., 199 (1986), 285.

31. A. M. Bond, M. Fleischmann, J. Robinson, J. Electroanal. Chem., 168 (1984), 299.

32. A. M. Bond, M. Fleischmann, J. Robinson, J. Electroanal. Chem., 172 (1984), 11.

33. C. Amatore, M. R. Deakin, R. M. Wightman, J. Electroanal. Chem., 220 (1987), 49.

34. K. B. Oldham, J. Electroanal. Chem., 250 (1988), 1.

35. I. Geng, A. G. Ewing, J. C. Jernigan, R. W. Murray, Anal. Chem., 58 (1986), 852.

36. M. J. Pena, M. Fleischmann, N. Garrard, J. Electroanal. Chem., 220 (1987), 31.

37. M. Ciszkowska, Z. Stojek, J. Electroanal. Chem., 213 (1986), 189.

38. J. C. Imbeaux, J. M. Savéant, J. Electroanal. Chem., 281 (1970), 325.

39. J. C. Imbeaux, J. M. Savéant, J. Electroanal. Chem., 31 (1971), 183.

40. D. F. Milner, M. J. Weaver, Anal. Chim. Acta., 198 (1987), 245.

41. S. Bruckenstein, Anal. Chem., 59 (1987), 2098.

42. K. B. Oldham, J. Electroanal. Chem., 237 (1987), 303.

43. C. G. Zoski, A. M. Bond, C. L. Colyer, J. C. Myland, K. B. Oldham, J. Electroanal. Chem., 263 (1989), 1.

44. L. K. Safford, M. J. Weaver, J. Electroanal. Chem., 261 (1989), 241.

45. A. R. Gourlay, J. Inst. Maths. Applics., 6 (1970), 375.

46. A. R. Gourlay, G. R. McGuire, J. Inst. Maths. Applics., 7 (1971), 216.

47. D. Britz, "Lecture Notes in Chemistry: Digital Simulation at Electrodes," Springer-Verlag, New York, 1981.

48. D. Shoup, A. Szabo, J. Electroanal. Chem., 140 (1982), 237.

49. D. Shoup, A. Szabo, J. Electroanal. Chem., 160 (1984), 1.

50. A. C. Michael, R. M. Wightman, C. A. Amatore, J. Electroanal. Chem., 267 (1989), 33.

51. R. S. Nicholson, I. Shain, Anal. Chem., 36 (1964), 706.

52. R. S. Nicholson, Anal. Chem., 37 (1965), 1351.

53. A. J. Bard, L. R. Faulkner, Electrochemical Methods: Fundamental Applications, John Wiley and Sons, Inc., (New York, 1980).

54. J. Newman, J. Electrochem. Soc., 113 (1966), 501.

55. K. M. Kadish, J. Q. Ding, T. Malinski. Anal. Chem., 56 (1984), 1741.

56. W. H. Press, B. P. Flannery, S. A. Teukolsky, W. T. Vetterling, Numerical Methods, Cambridge University Press, (New York, 1989).

57. D. O. Wipf, A. C. Michael, R. M. Wightman, J. Electroanal. Chem., 269 (1989), 15.

FIGURE CAPTIONS

Fig. 1

Plots of cyclic voltammetric peak separations, ΔE_p observed at a 5 μm radius (dashed traces) and a 0.5 μm radius (solid traces) microdisk, assuming $D = 10^{-5}$ cm^2 s^{-1} n = 1, T = 298°K, versus log($\nu^{-1/2}$) for several different heterogeneous rate constants; k_s (cm^{-1}): ∞, asterisks; 5, inverted triangles; 2, diamonds; 1, upright triangles; 0.5, squares; 0.2, circles. Open symbols for $k_s = \infty$ (squares), and $k_s = 0.2$ cm s^{-1} (circles).

Fig. 2

Plots of ΔE_p versus log(σ) for the following values of the dimensionless kinetic parameter ψ. ∞, crossed inverted triangles; 10, crossed upright triangles; 5, crossed squares; 2, crossed circles; 1, plus signs; 0.5, inverted open triangles; 0.2, open diamonds; 0.1, upright open triangles; 0.05, open squares; 0.02, open circles.

Fig. 3

Voltammetric waveshapes (for $k_s \rightarrow \infty$) seen under different diffusional conditions at a microdisk, for the specific σ values indicated.

Fig. 4

Plots of ($E_{1/4} - E_f$) versus log($\nu^{-1/2}$) for several different rate constants. Symbols and conditions are as in Fig. 1.

Fig. 5

Plots of ($E_{1/4} - E_f$) versus log(σ) for a series of values of ψ. Symbols are as in Fig. 2.

Fig. 6

Plots of ΔE_p versus log($\nu^{-1/2}$) for voltammograms generated for $k_s \rightarrow \infty$ but with nonzero solution resistivities, ρ_Ω (Ω - cm) as follows: $\rho_\Omega = 0$, asterisks; 200, inverted triangles; 450, diamonds; 725, upright triangles; 1800, squares; 2670, circles. Reactant concentration (C_R) was 2 x 10^{-3} M. Other conditions as in Fig. 1.

Fig. 7

Plots of ($E_{1/4} - E_f$) versus log($\nu^{-1/2}$) for voltammograms generated for conditions as in Fig. 6.

Fig. 8

Plots of $\Delta\xi_p$ versus log(σ) for a series of different values of the dimensionless resistive parameter, ρ, as follows: $\rho = 0$, asterisks; 0.1, closed circles; 0.2, open squares; 0.5, inverted closed triangles; 1.0, closed diamonds; 2.0, upright closed triangles; 5.0, closed squares; 10, open circles.

Fig. 9

Plots of ($\xi_{\frac{1}{2}} - \xi_r$) versus log($\sigma$) for a series of different values of ρ. Symbols and conditions are as in Fig. 8.

Fig. 10

Plots of ΔE_p versus log($\nu^{-\frac{1}{2}}$) for a 5 μm radius electrode with conditions in Fig. 3 for ρ_Ω = 725 Ω-cm (open symbols) and 1800 Ω-cm (closed symbols), with C_{dl} = 5 μF cm^{-2} (circles), 15 μF cm^{-2} (squares) and 25 μF cm^{-2} (triangles). Reactant concentration (C_R) was 2 x 10^{-3} M, diffusion coefficient (D) = 1 x 10^{-5} cm^2 s^{-1}

Fig. 11

Plots of ($E_{\frac{1}{2}} - E_r$) versus log($\nu^{-\frac{1}{2}}$) for conditions as in Fig. 10.

Fig. 12

Plots of ΔE_p versus log($\nu^{-\frac{1}{2}}$) for conditions as follows: a = 0.5 μm (solid traces), 5 μm (dashed traces); k_s = 0.2 cm s^{-1}, (circles), 5.0 cm s^{-1} (squares), ρ_Ω = 100 Ω-cm (open symbols), 1000 Ω-cm (closed symbols). Other conditions: C_{dl} = 5 μF cm^{-2}, n = 1, T = 298°K, D = 10^{-5} cm^2 s^{-1}, C° = 2 x 10^{-3}M.

Fig. 13

Plots of ($E_{\frac{1}{2}} - E_r$) versus log($\nu^{-\frac{1}{2}}$) for conditions as in Fig. 12.

Fig. 14

Plots of ΔE_p versus log($\nu^{-\frac{1}{2}}$) for conditions as follows: a = 0.5 μm (solid traces), 5 μm (dashed traces); C_{dl} = 25 μF cm^{-2} (squares), 5 μF cm^{-2} (circles), ρ_Ω = 100 Ω-cm (open symbols), 1000 Ω-cm (closed symbols). Other conditions: k_s = 0.2 cm s^{-1}; C_R = 2 x 10^{-3}M, D = 10^{-5} cm^2 s^{-1}, n = 1, T = 298°K.

Fig. 15

Plots of ($E_{\frac{1}{2}} - E_r$) versus log($\nu^{-\frac{1}{2}}$) for conditions as in Fig. 14.

Fig. 16

Ratio of "apparent" to actual rate constant, k_s(app)/k_s, versus log ($\nu^{-\frac{1}{2}}$) for the following conditions: a = 5 μm, n = 1, T = 298°K, ρ_Ω = 200 Ω-cm, C_{dl} = 10 μF cm^{-2}, C° = 2 x 10^{-3}M, D = 10^{-5} cm^2 s^{-1}, k_s = 0.5 cm s^{-1} (circles), 0.2 cm s^{-1} (squares), 0.1 cm s^{-1} (triangles). The k_s(app) values were extracted from the simulated voltammograms by ignoring solution resistance effects (see text).

Fig. 17

Cyclic voltammograms simulated for $k_s \rightarrow \infty$ and 0.2 cm s^{-1} at sweep rates of (a) 2500 V s^{-1} and (b) 25 V s^{-1}. General conditions are: a = 5 x 10^{-4}

cm, $D = 1 \times 10^{-5}$ cm^2 s^{-1}, $C_{dl} = 10$ μF cm^{-2}, $C_o = 2 \times 10^{-3}$ M. In (a), solution resistivities (ρ_Ω) are: 0 (solid traces), 130 (dashed traces), and 720 Ω cm (dotted traces). The inner and outer trio of voltammograms refer to $k_s \rightarrow \infty$, and $k_s = 0.2$ cm s^{-1}, respectively. In (b), solid and dotted traces refer to $k_s \rightarrow \infty$ and $k_s = 0.2$ cm s^{-1}, respectively (curves for all resistivities above are essentially coincident - see text).

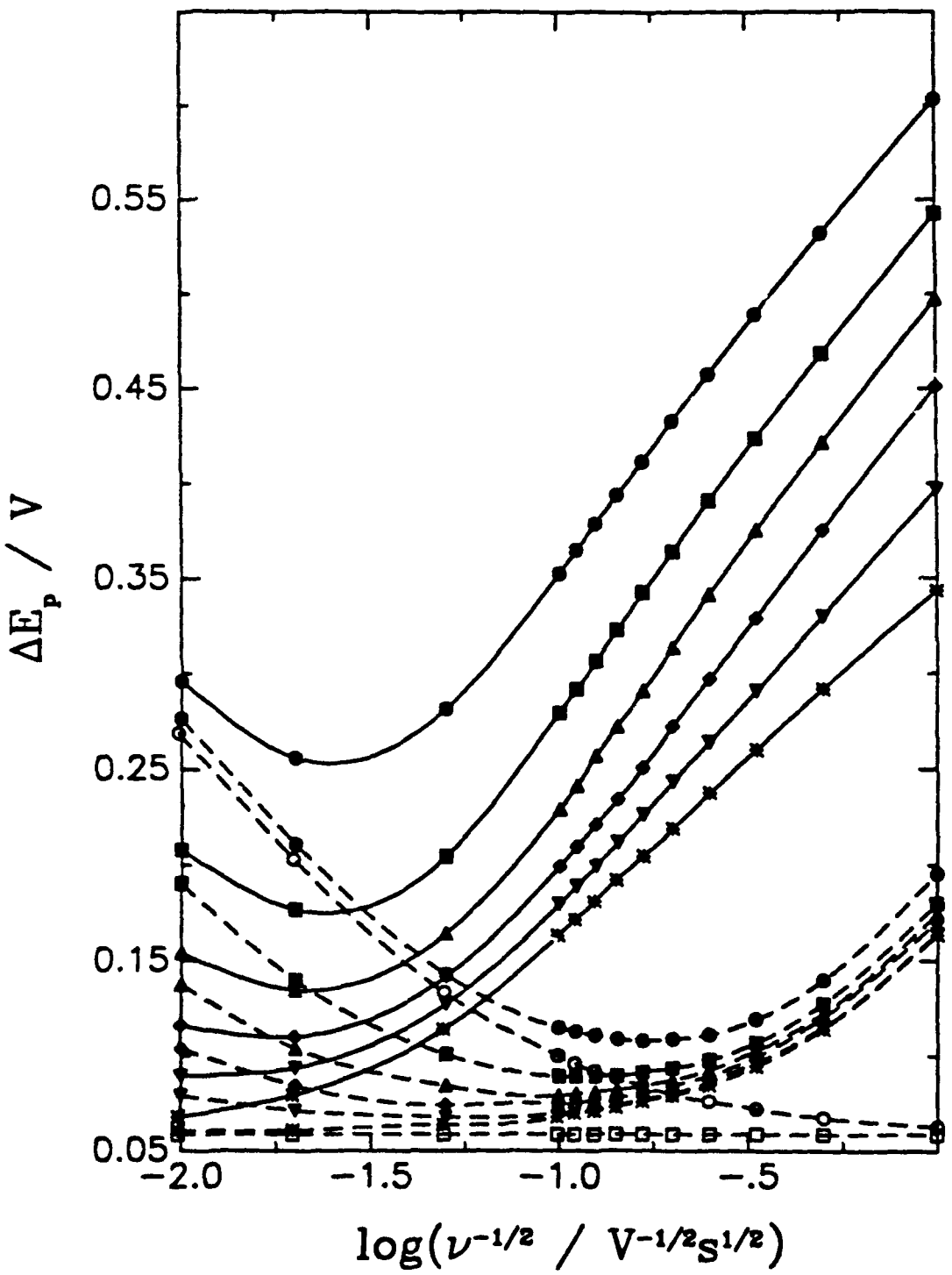

Fig. 1

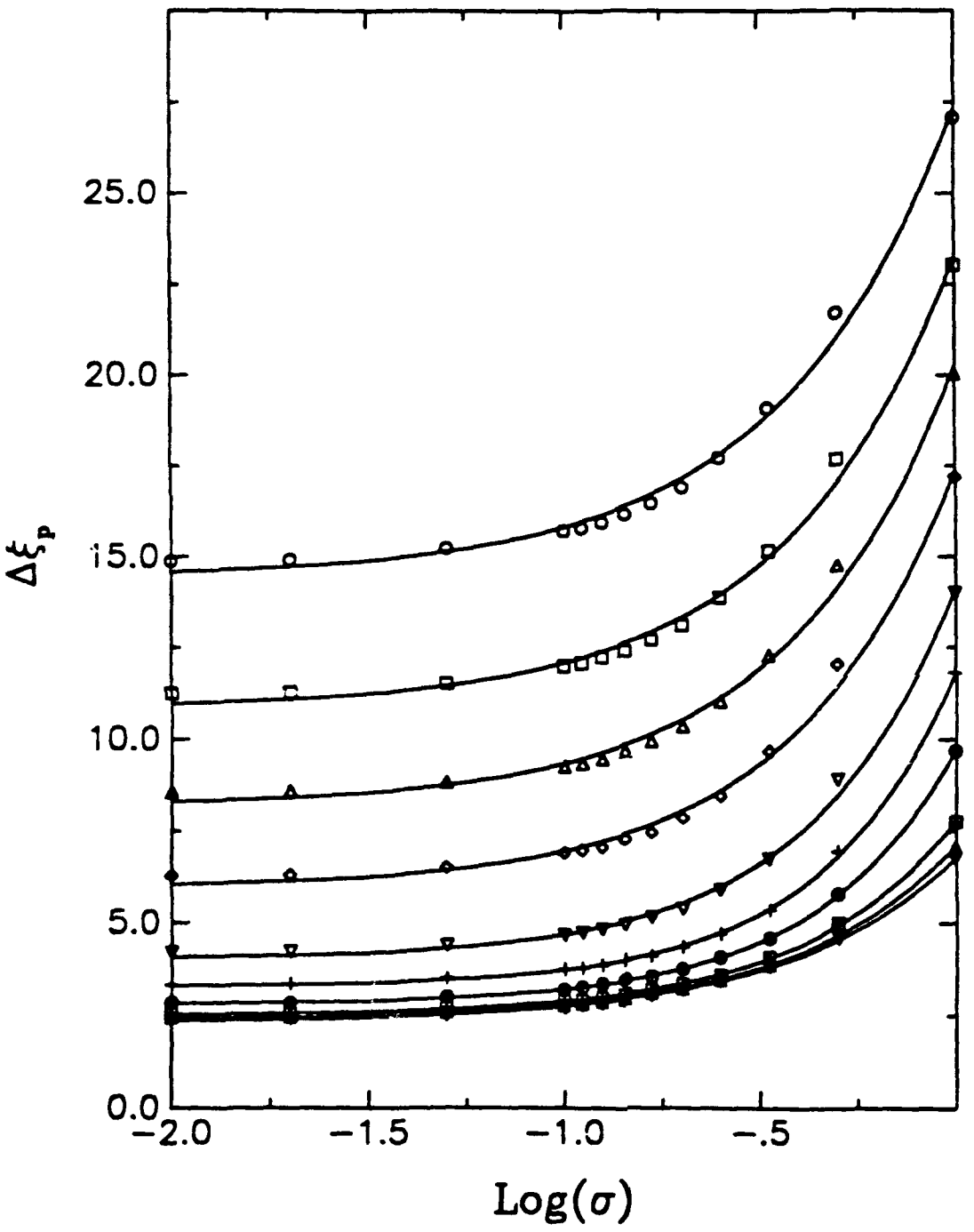

Fig. 2

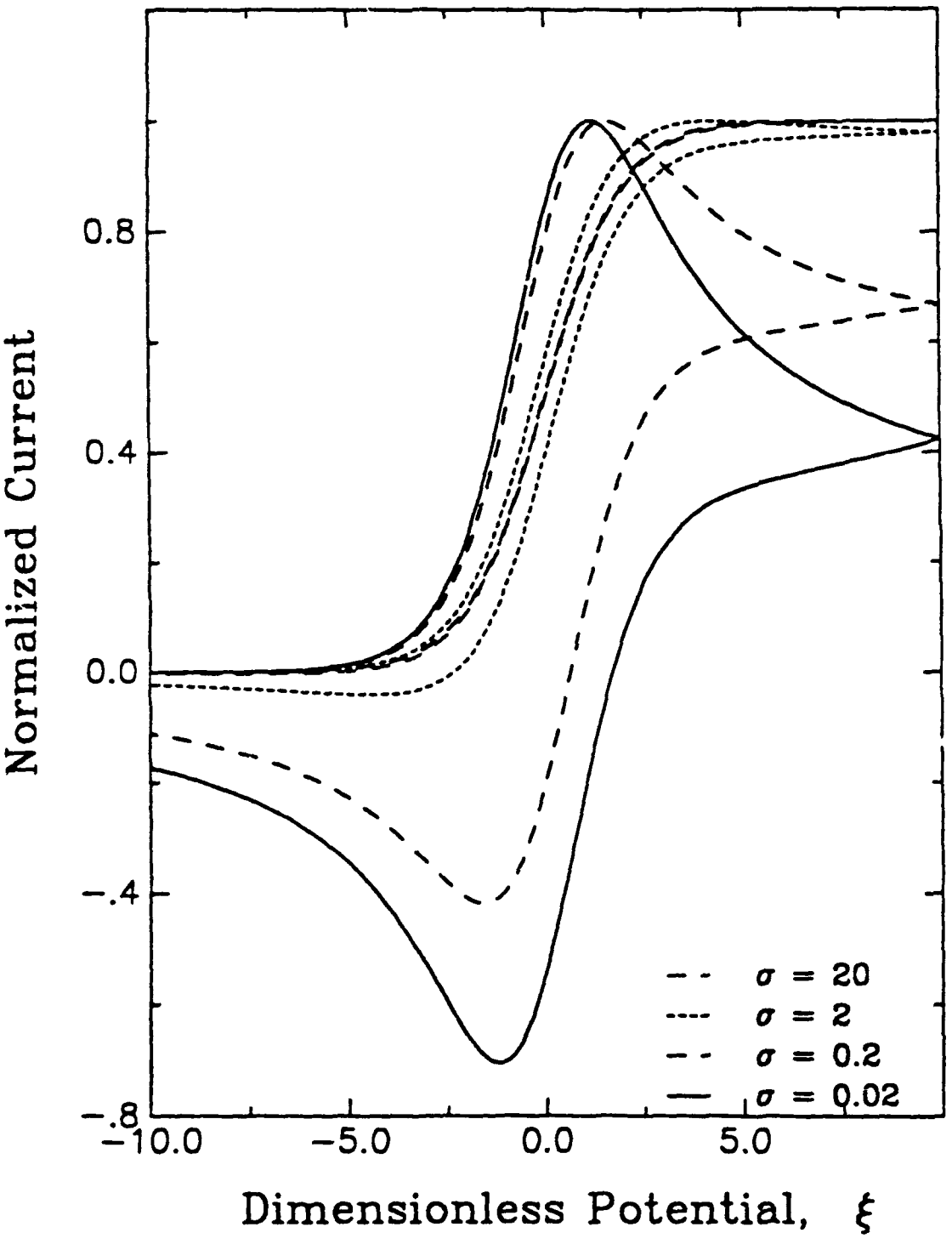
Normalized Current
0.8
0.4
0.0
-.4
-.8
−10.0
−5.0
0.0
5.0
Dimensionless Potential, ξ
σ = 20
σ = 2
σ = 0.2
σ = 0.02

Fig. 3

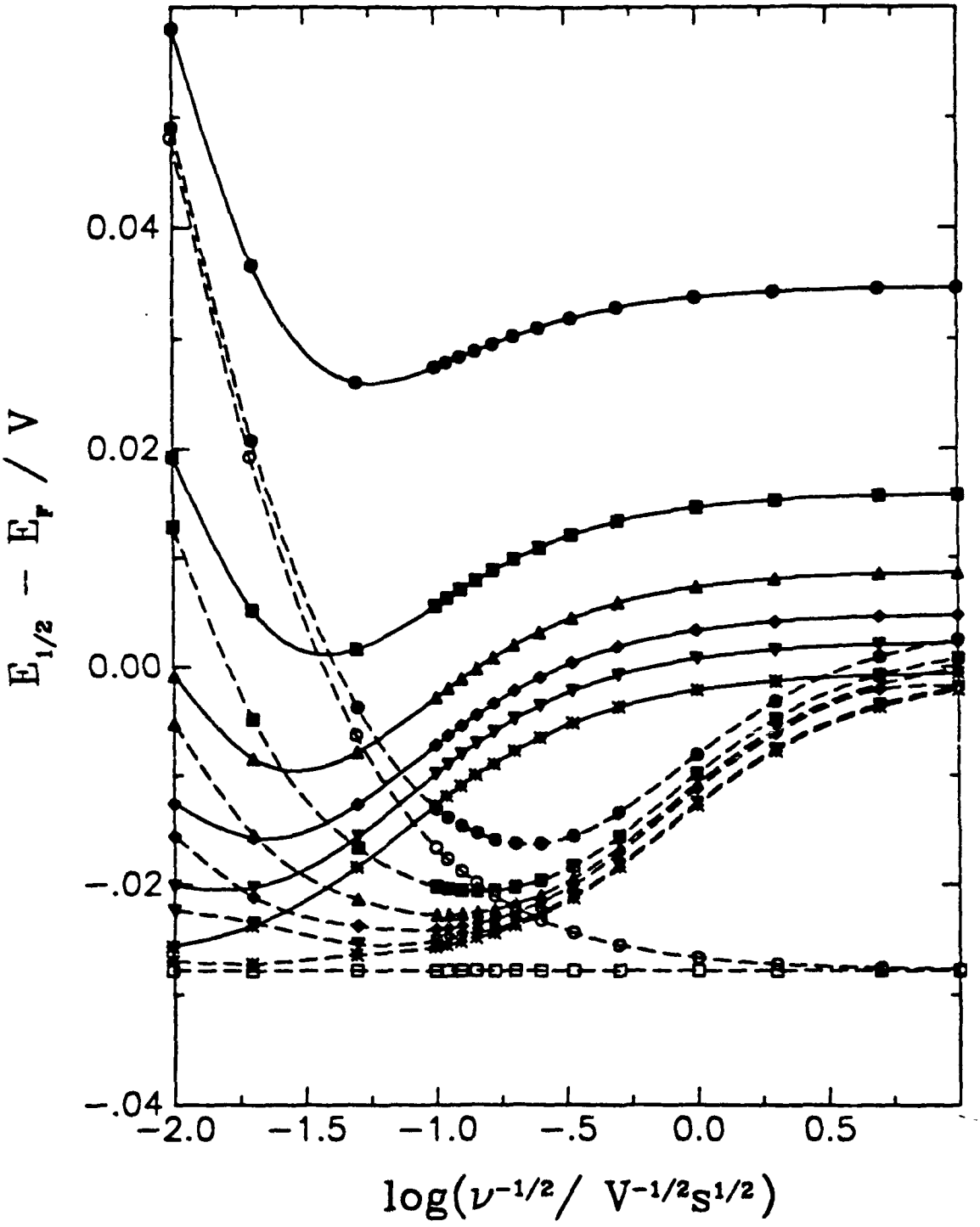

Fig. 4

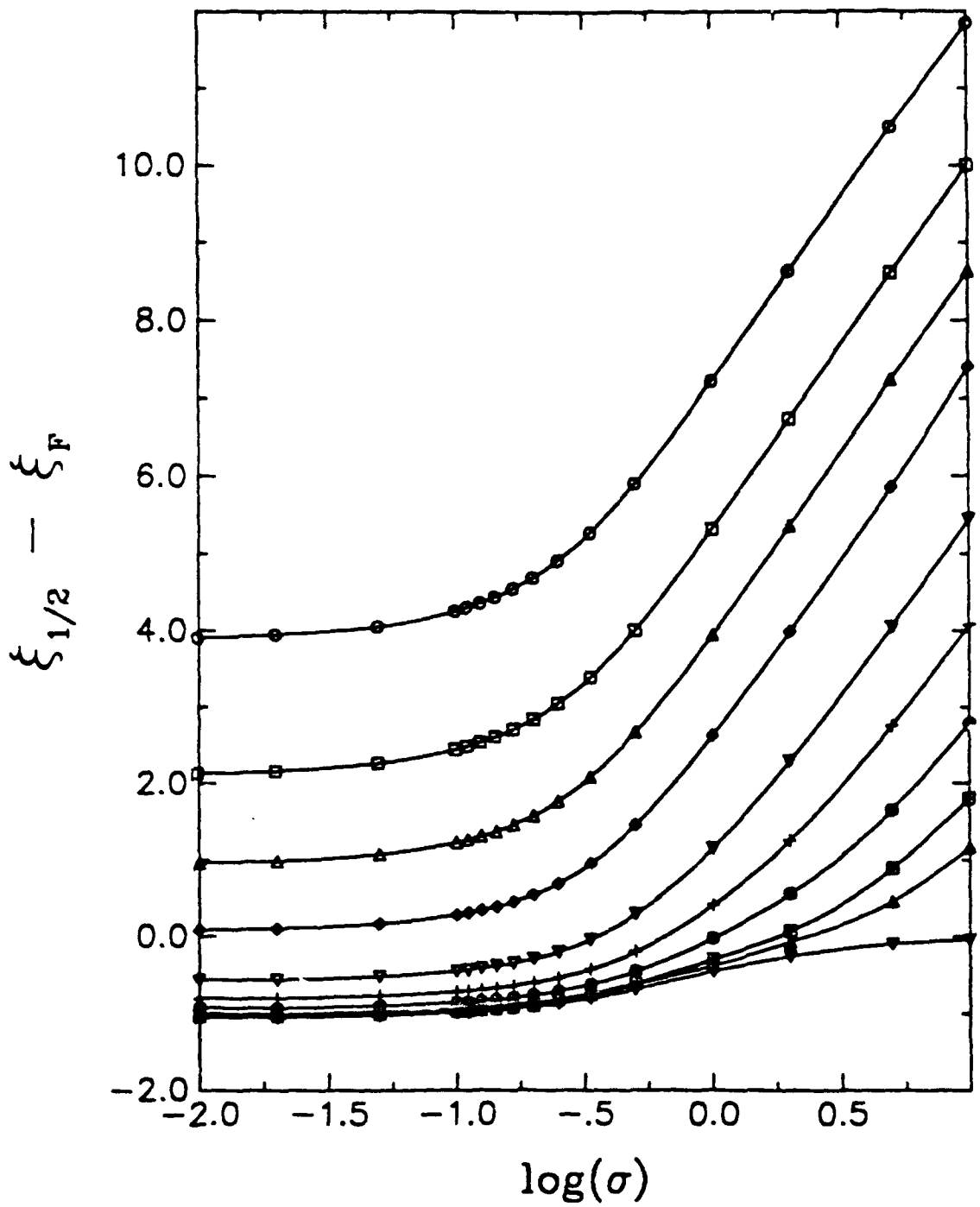

Fig. 5

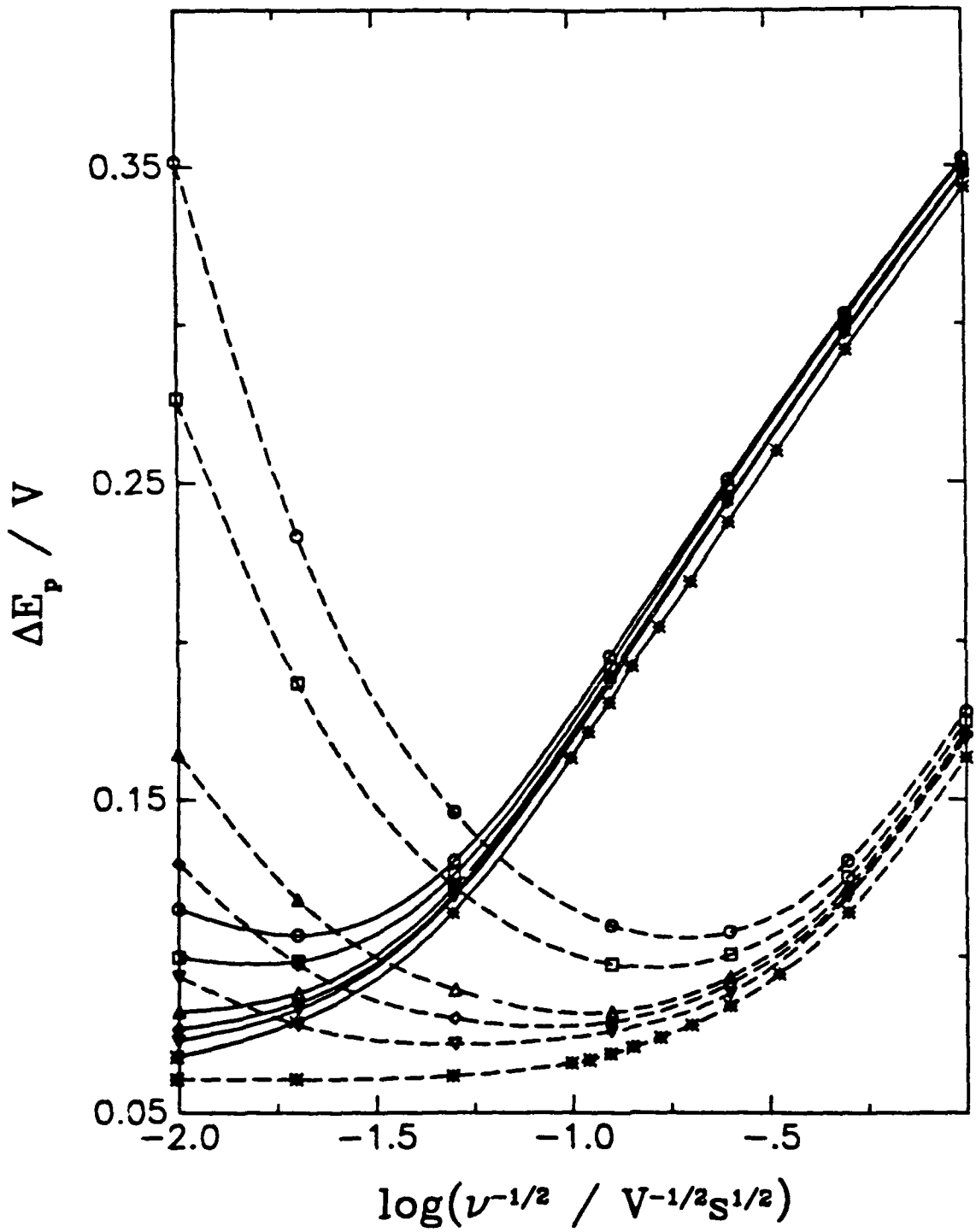

FIG 6

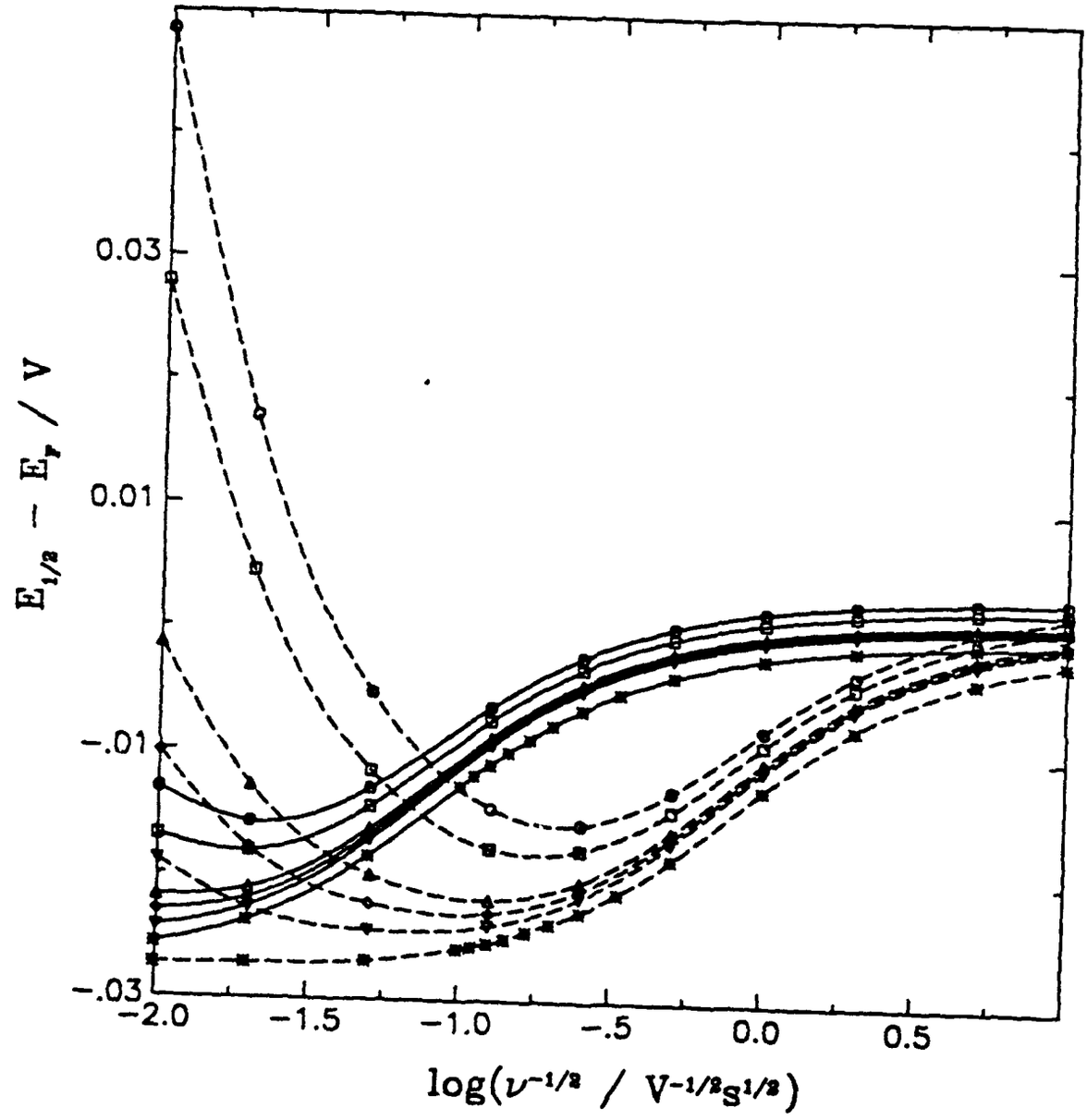

FIG 7

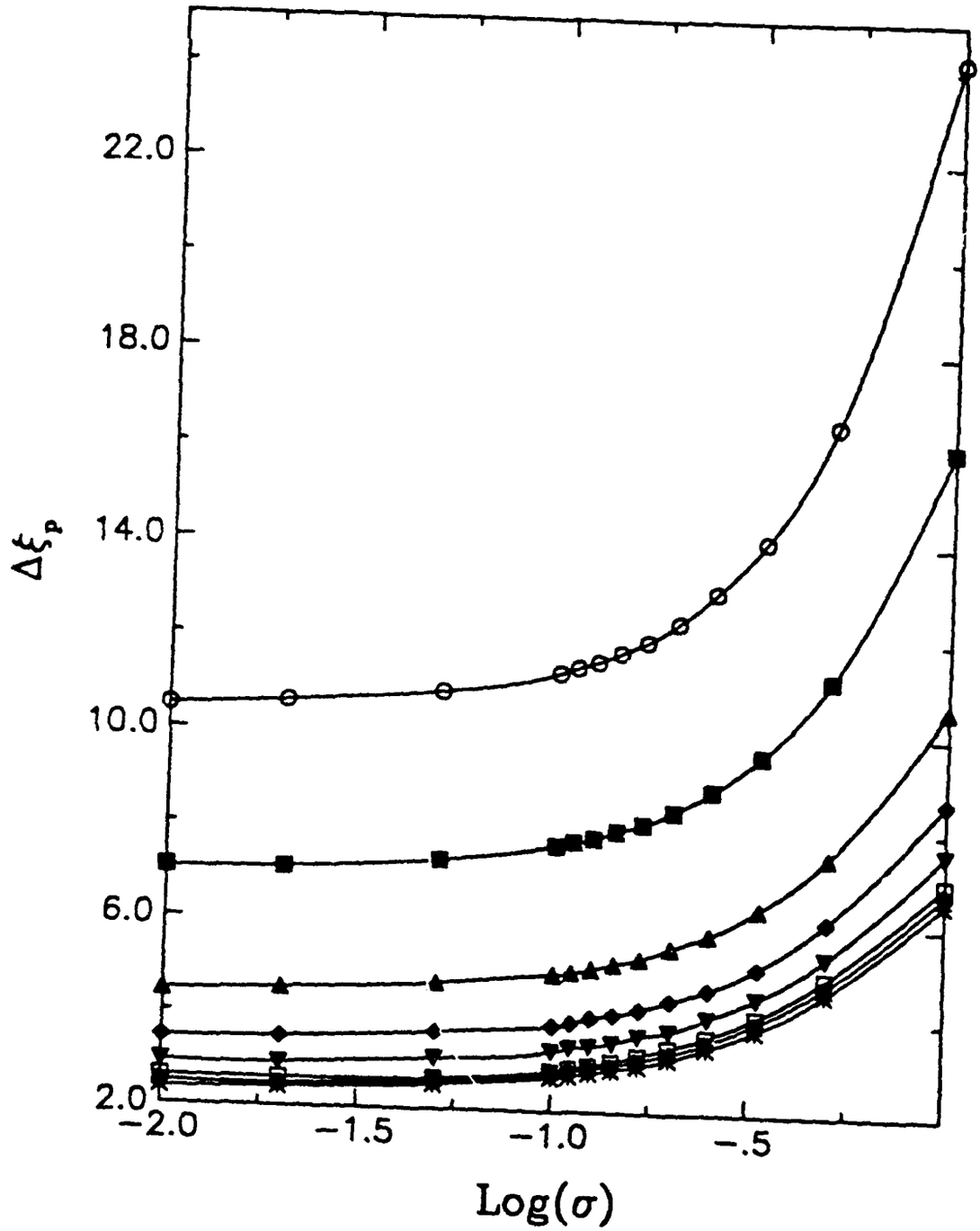

FIG 8

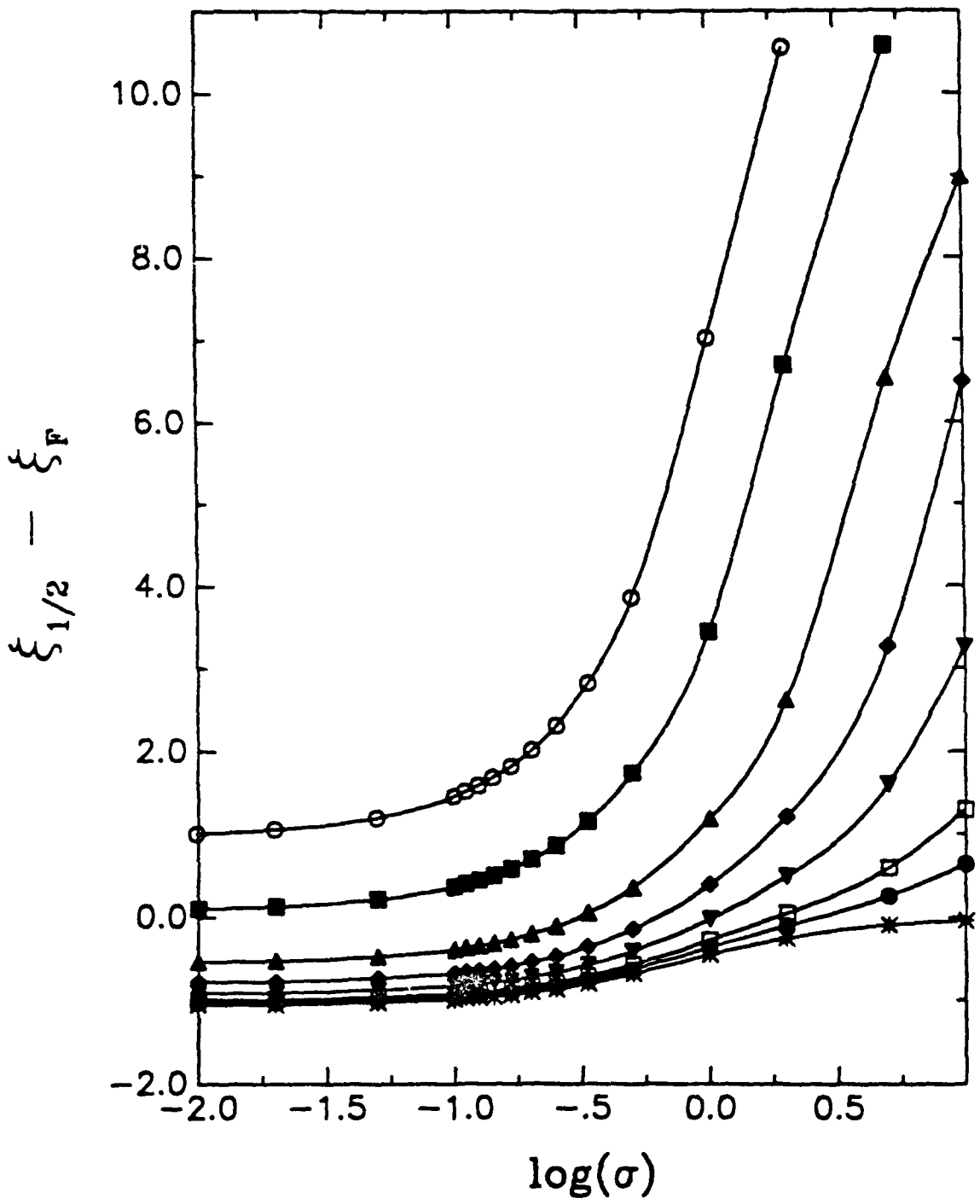

Fig. 9

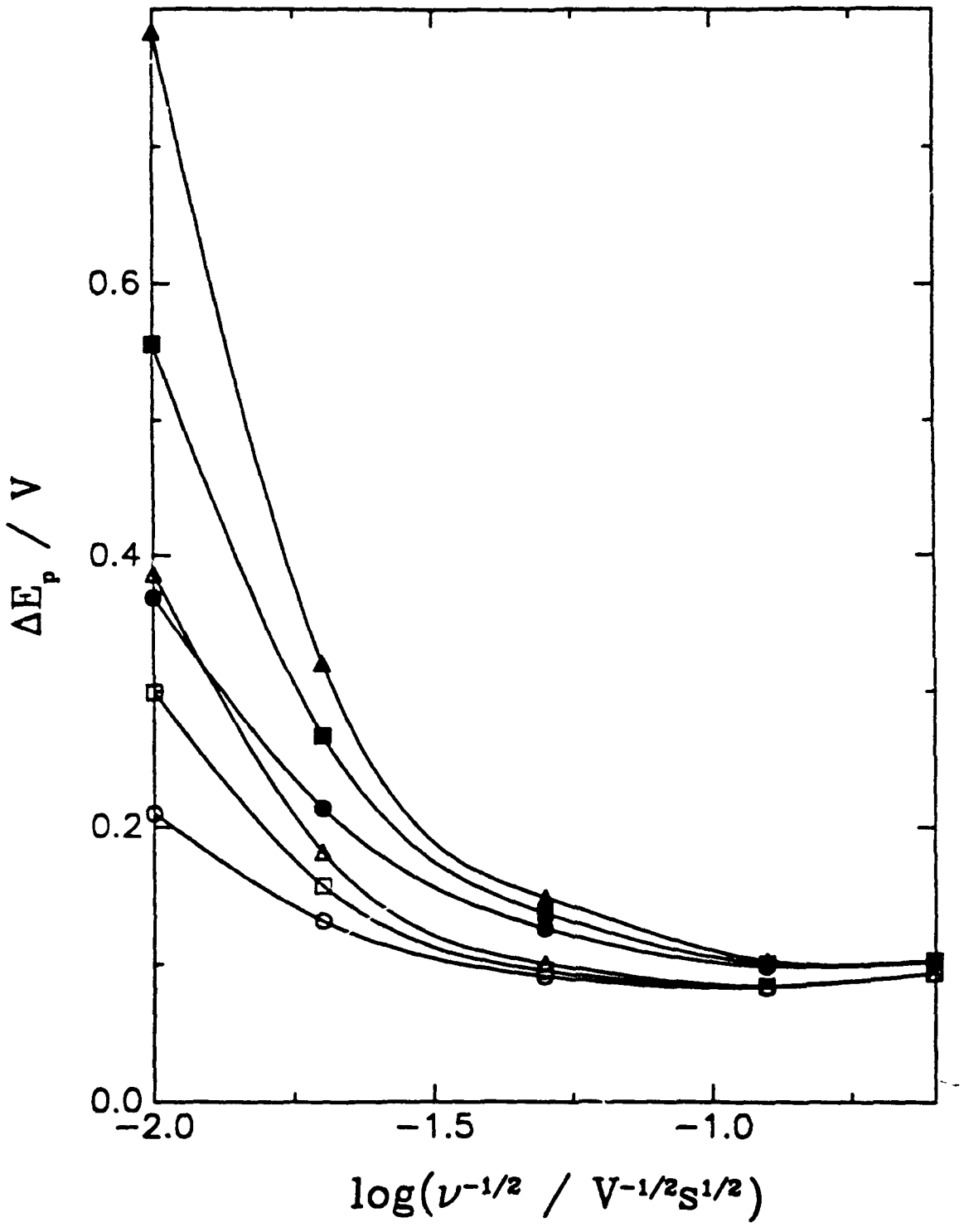

Fig. 10

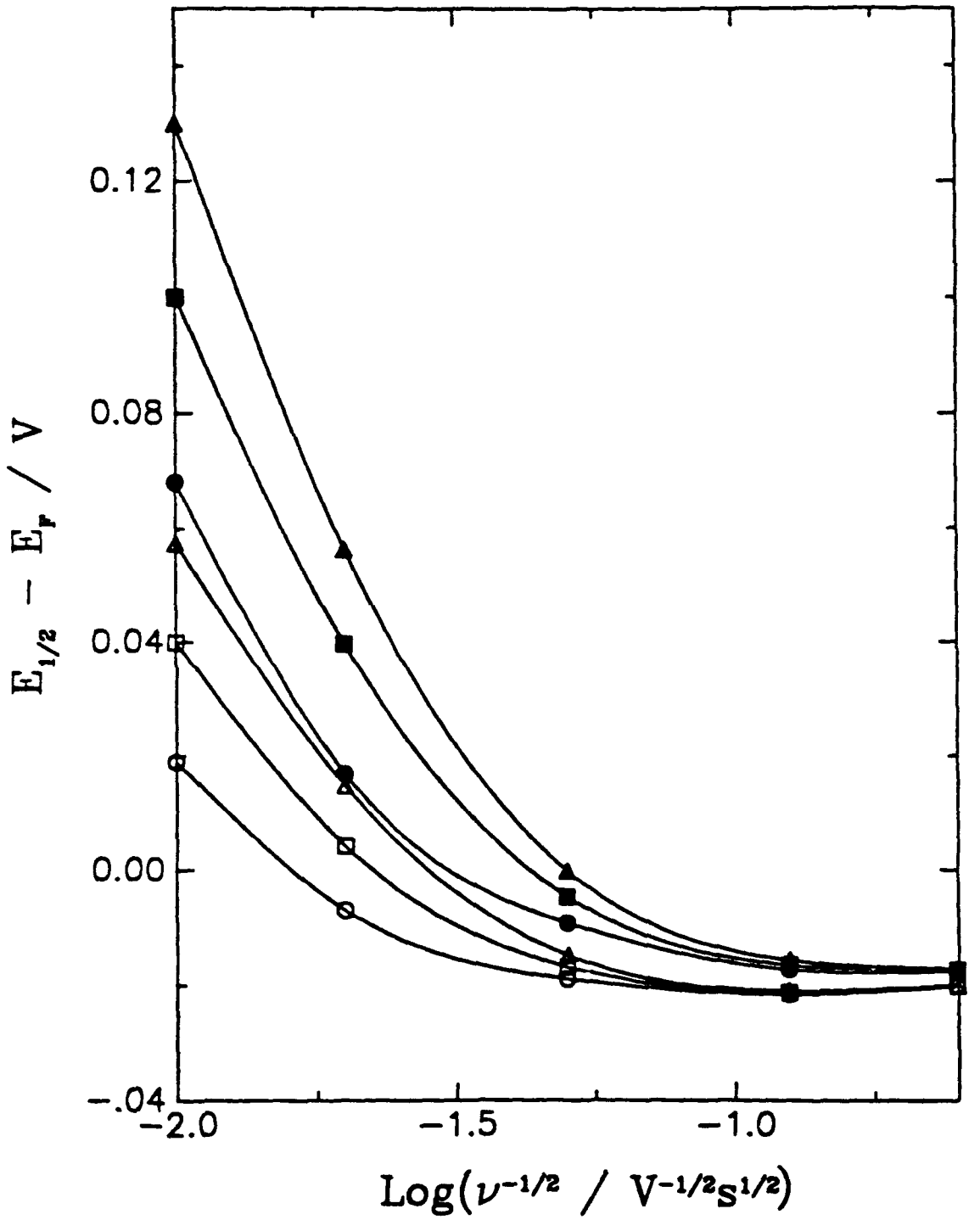

Fig. 11

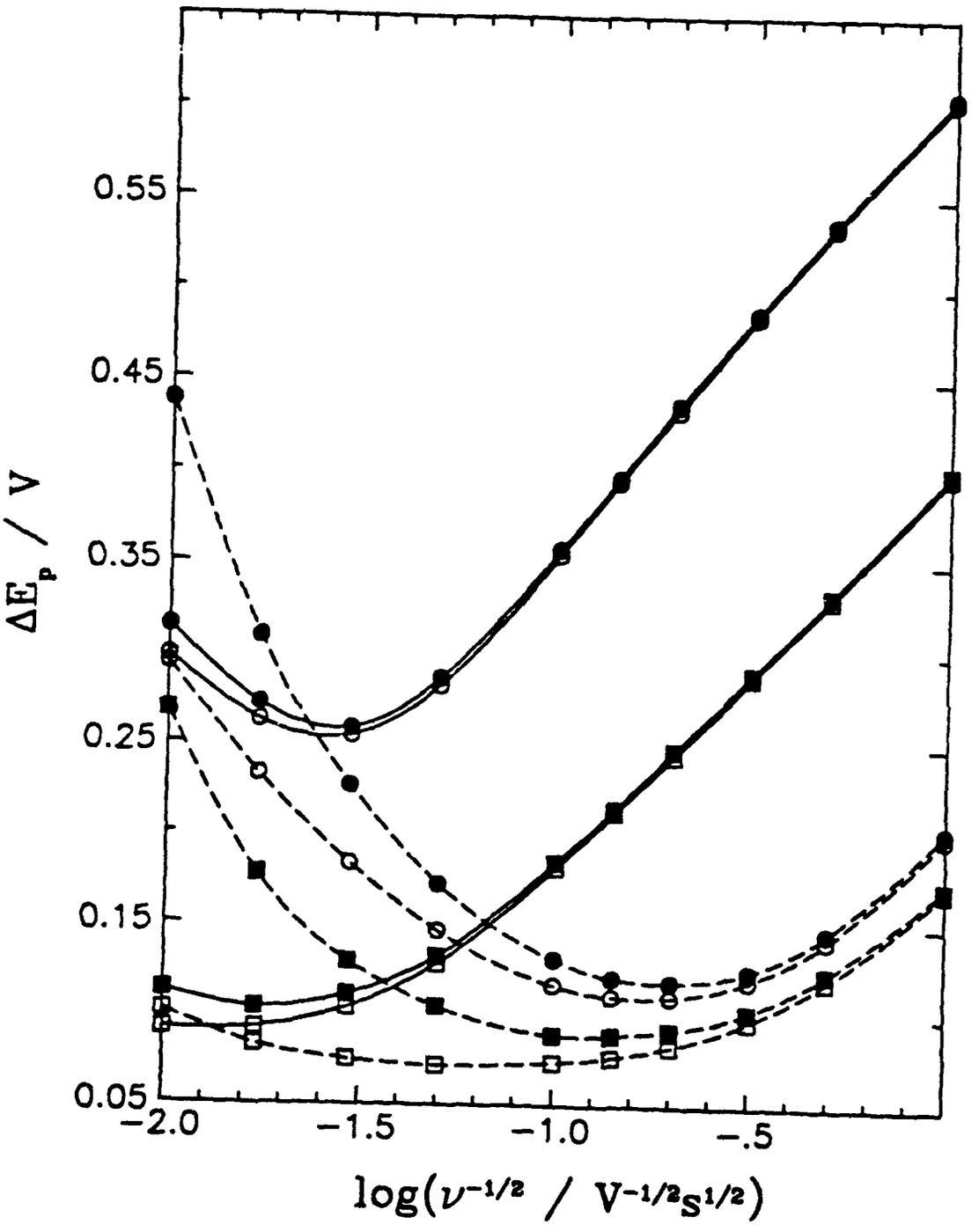

Fig. 12

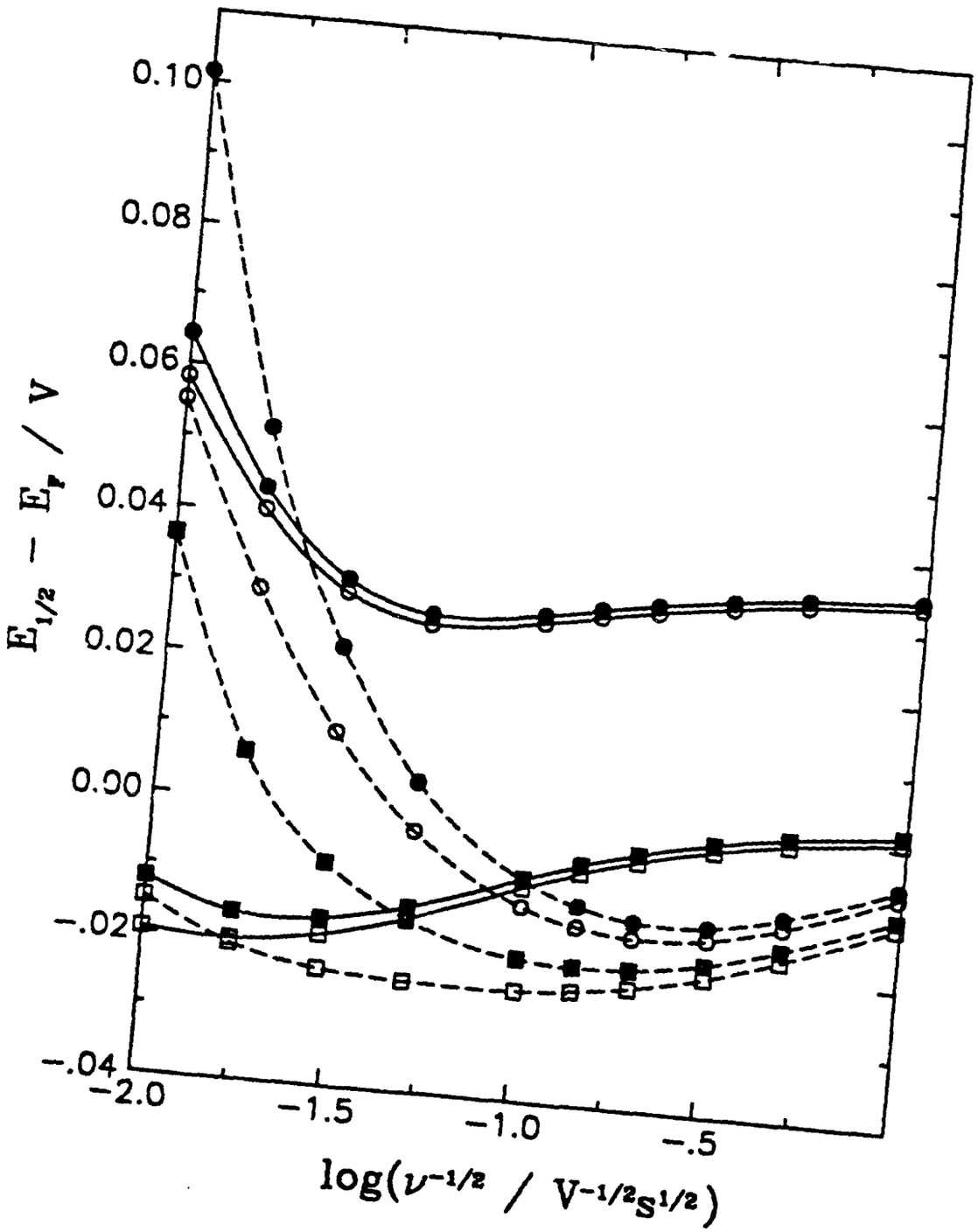

Fig. 13

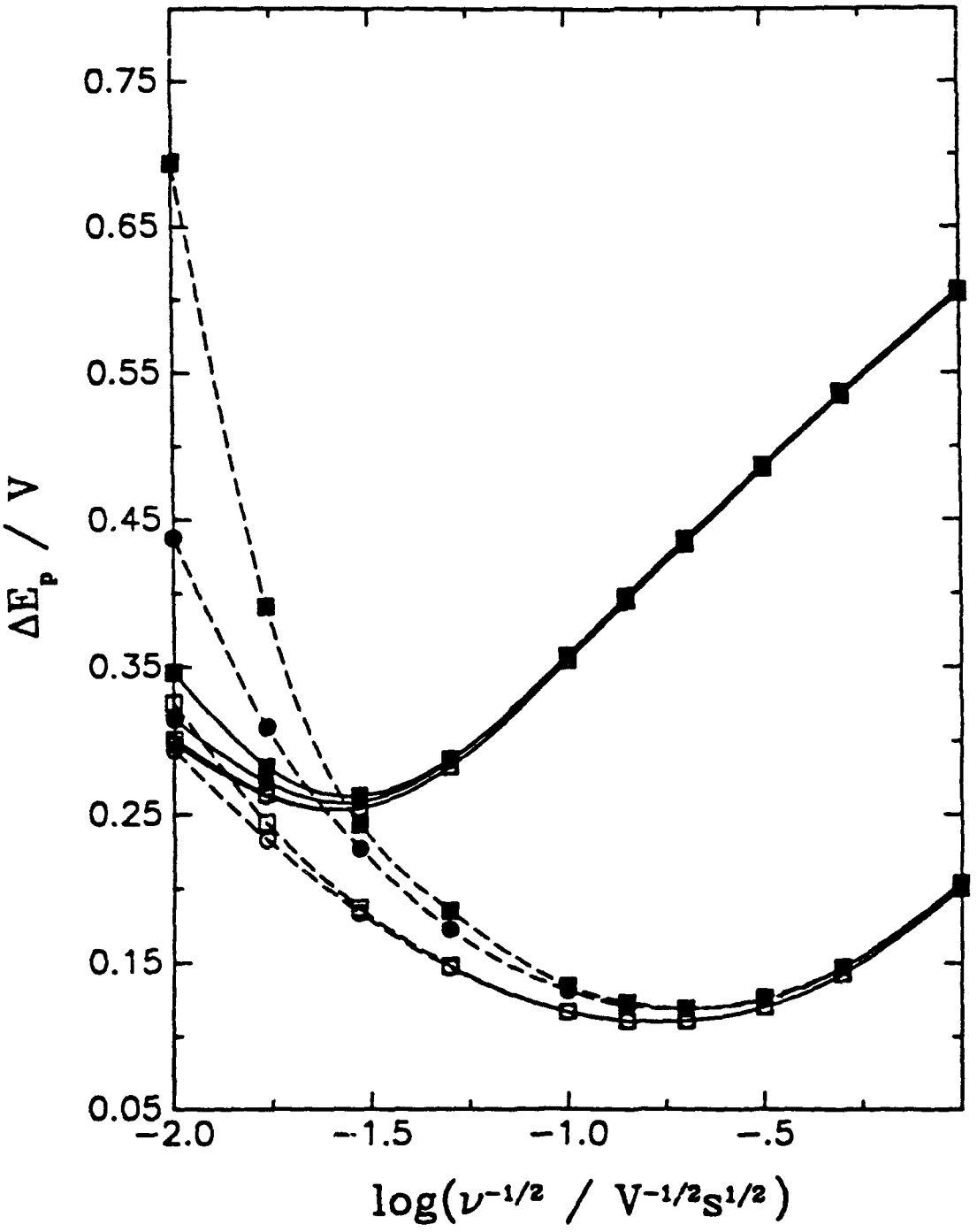
0.75
0.65
0.55
0.45
0.35
0.25
0.15
0.05
−2.0
−1.5
−1.0
−.5
ΔE_p / V
$\log(\nu^{-1/2} / V^{-1/2}s^{1/2})$

Fig. 14

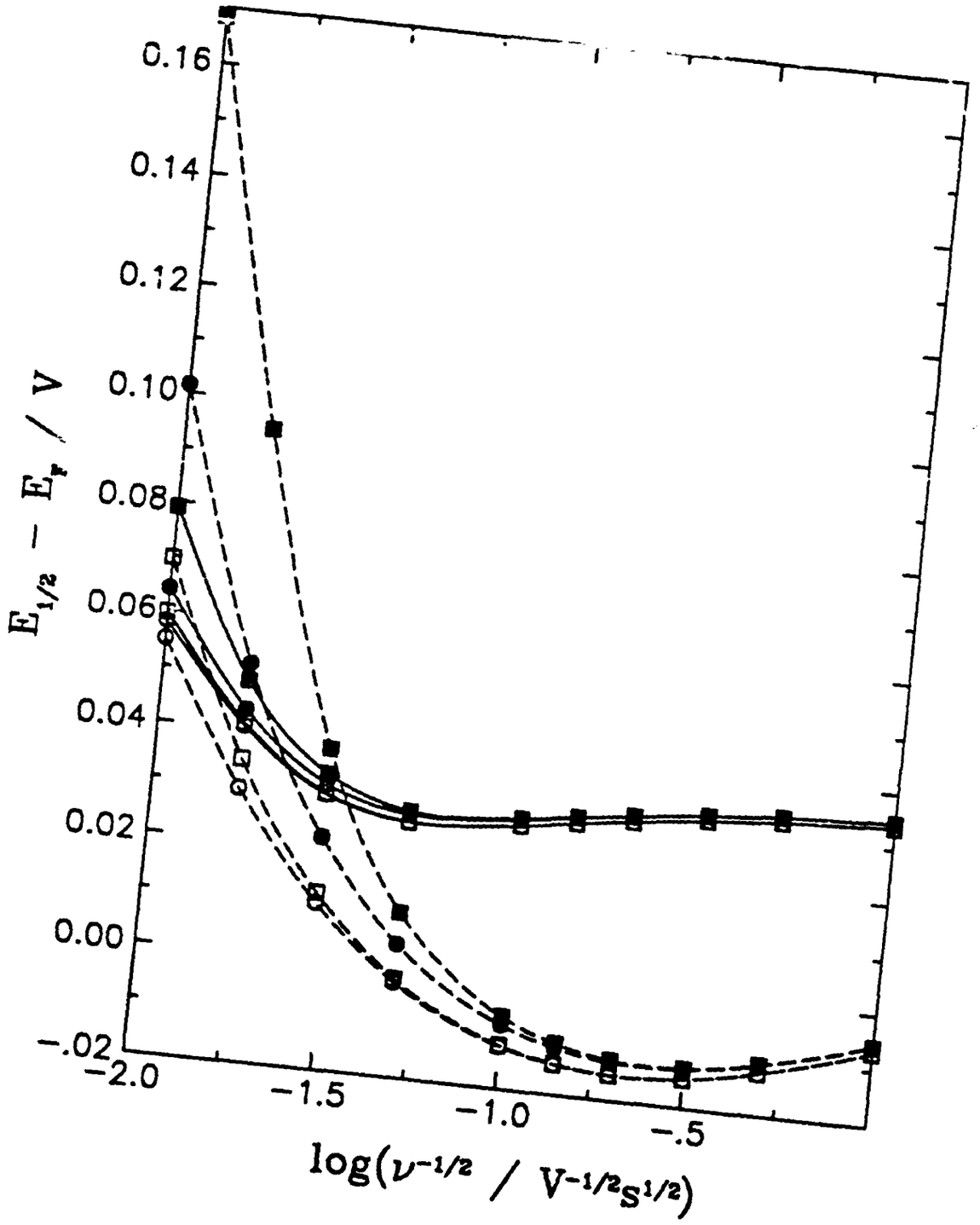
0.16
0.14
0.12
0.10
0.08
0.06
0.04
0.02
0.00
-.02
$E_{1/2} - E_r$ / V
-2.0
-1.5
-1.0
-.5
$\log(\nu^{-1/2} / V^{-1/2}S^{1/2})$

Fig. 15

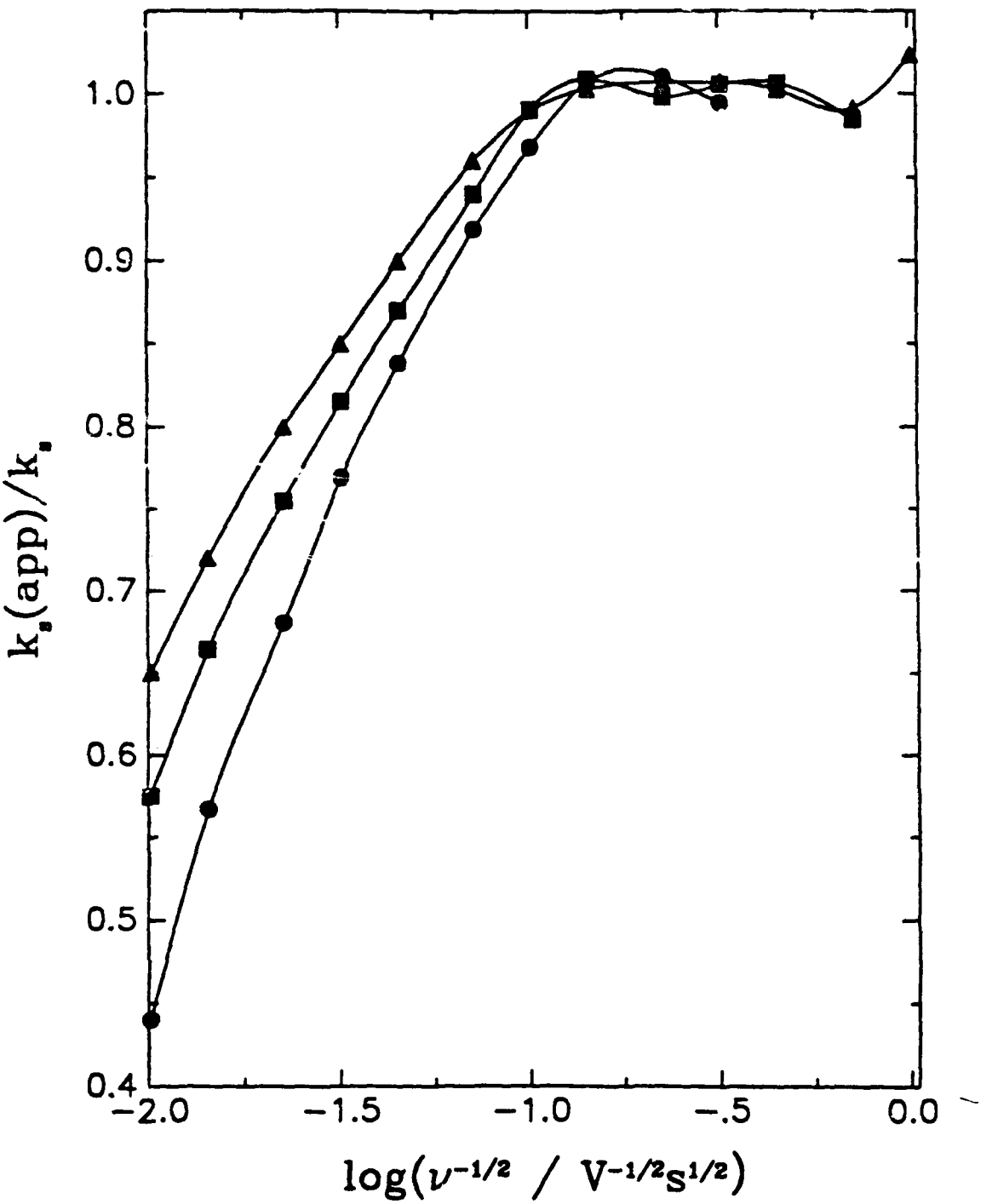

Fig. 16

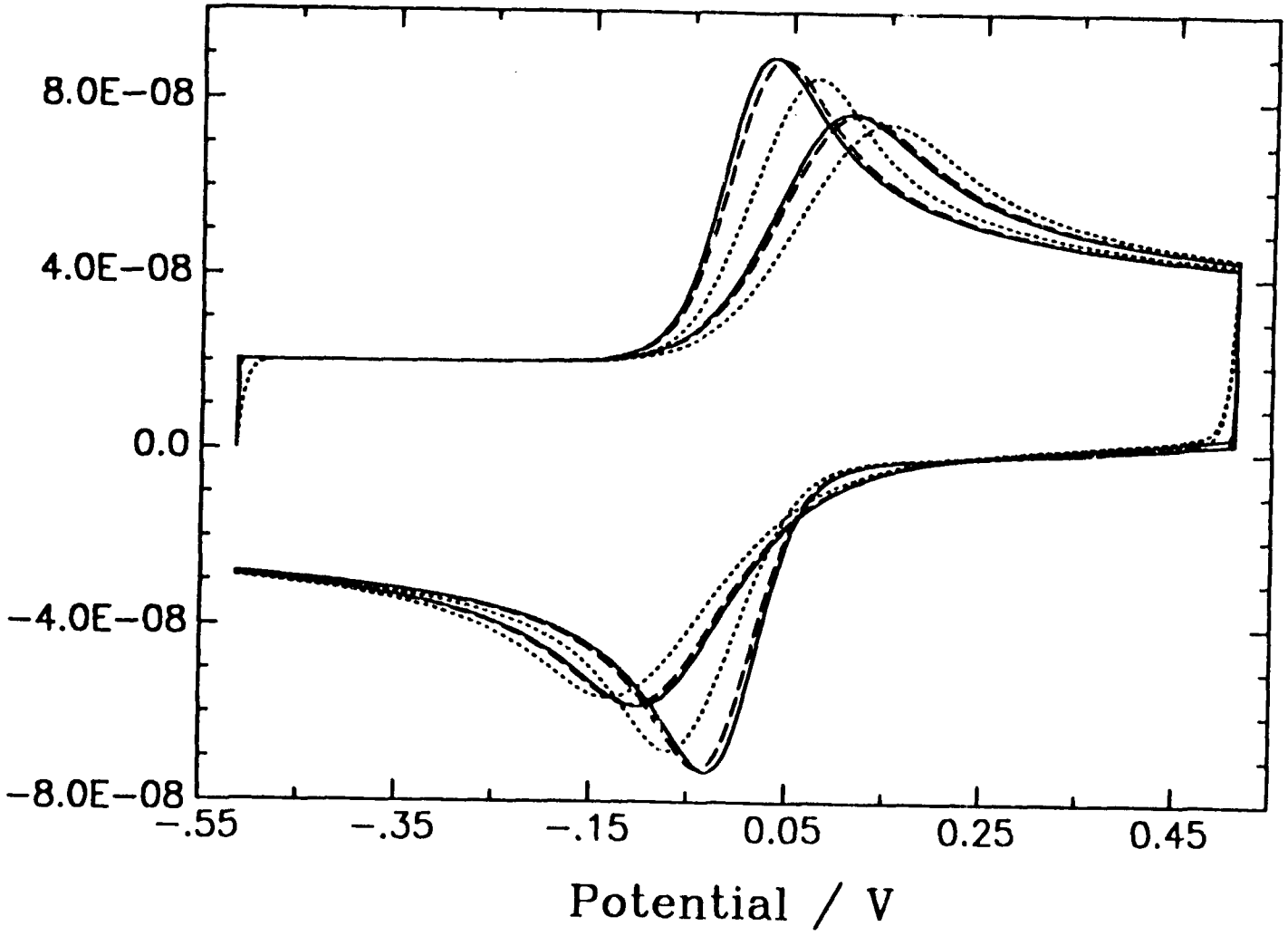
8.0E−08
4.0E−08
0.0
−4.0E−08
−8.0E−08
Current / A
−.55
−.35
−.15
0.05
0.25
0.45
Potential / V

Fig. 17a

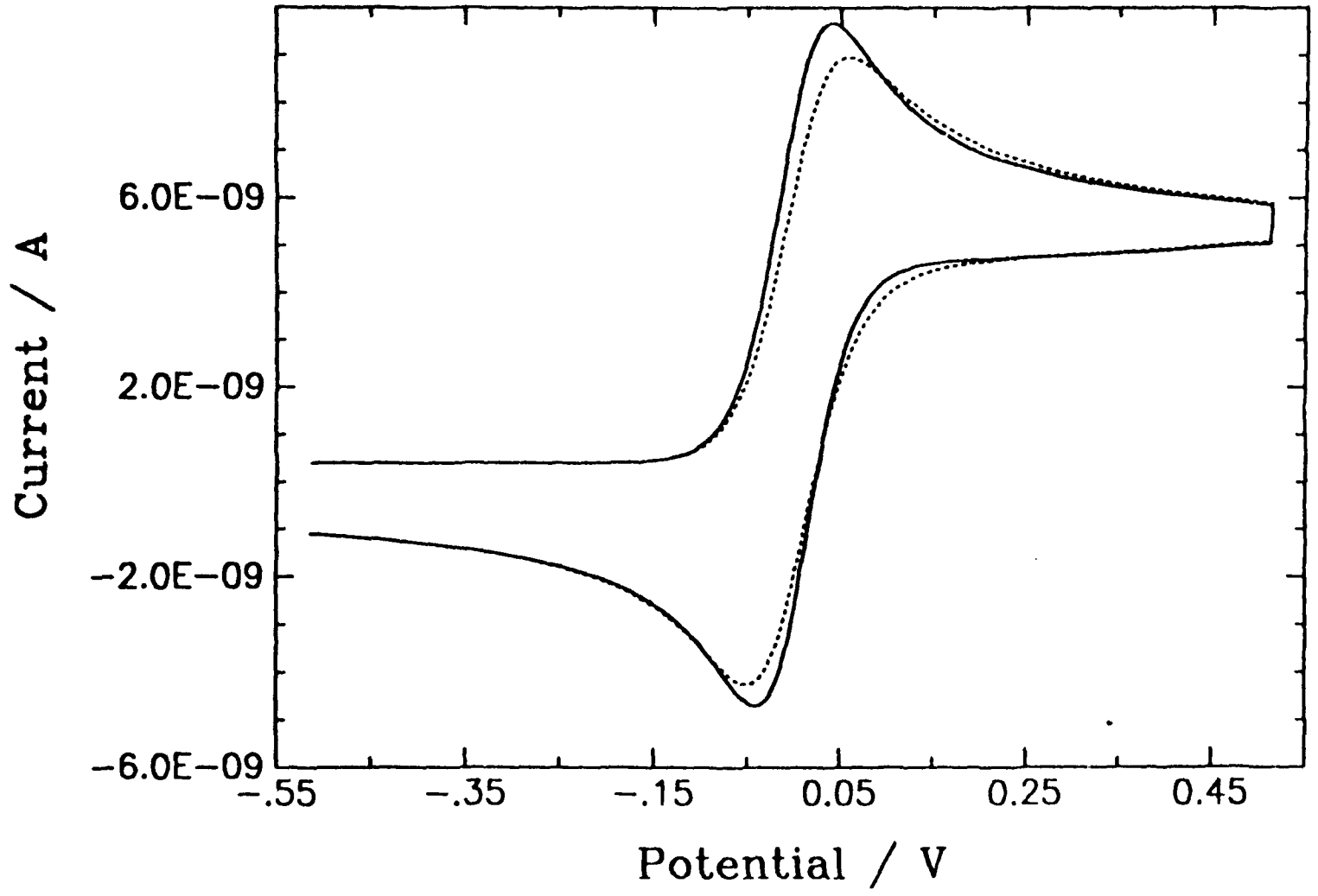
Current / A
6.0E−09
2.0E−09
−2.0E−09
−6.0E−09
−.55
−.35
−.15
0.05
0.25
0.45
Potential / V

Fig. 17b